

Ho Chi Minh City University of Science
Department of Theoretical Physics
Bachelor's Degree Thesis

THE SCATTERING PROCESS

$$e^{-} + e^{+} \longrightarrow f + \bar{f}$$

WITH QED CORRECTION



Thesis Supervisor: Dr. LE Duc Ninh
Student: PHAN Vo Hong Minh

Acknowledgement

First, I would like to send a special thank you to my family (mom, dad, Tu, and Hon) for always backing me on the way to my dream to become a scientist.

Also, thank you to all my teachers at the Department of Theoretical Physics (thầy Phong, thầy Tuyên, thầy Nhã, thầy Khiêm, thầy Châu, and thầy Hà) and my Physics teachers in high school (thầy Diễm and cô Lan Anh). Indeed, your instructive and inspirational lectures ignited my passion for science which in turn gave me strength and courage to cope with difficulties both in science and in my life.

For my friends, a big thank you for your hilarious jokes that helped me to overcome stress and other not-so-happy stuff in my life. Besides, group discussion with you guys was a great way to somehow sharpen my learning skills and gain more knowledge not only in Physics but also in many other interesting fields of science.

Finally, I wish express my sincere gratitude to thầy Ninh-my thesis supervisor for continuously supporting and encouraging me during the time I am working on my thesis. Certainly, you gave me great motivation and strengthened my determination to keep on learning and pursuing a career in Theoretical Physics.

July 15, 2016

PHAN Vo Hong Minh.

Contents

Acknowledgement	1
Introduction	3
1 The scattering process $e^- + e^+ \rightarrow \mu^- + \mu^+$ in QED	4
1.1 An overview of QED	4
1.1.1 The general photon propagator	5
1.1.2 The vertex factor of QED	6
1.2 The Feynman amplitude	7
1.3 Several physical quantities of interest	10
1.3.1 The differential cross-section and the total cross-section	10
1.3.2 Angular distribution of muon	11
1.3.3 Transverse momentum and longitudinal momentum distributions of muon	11
1.3.4 Rapidity and pseudo-rapidity distributions of muon	13
2 The scattering process $e^- + e^+ \rightarrow \mu^- + \mu^+$ in SM	16
2.1 An overview of SM	16
2.1.1 The fermionic term of SM Lagrangian	17
2.1.2 The gauge fields in SM	18
2.2 The vertex factor of Z -boson	18
2.2.1 The neutral part of the covariant derivative	19
2.2.2 Left-handed electrons	19
2.2.3 Right-handed electrons	20
2.2.4 The vertex factor of eeZ	21
2.3 The propagator of Z -boson	22
2.4 The Feynman amplitude	23
2.4.1 The forward-backward asymmetry	26
2.4.2 Transverse momentum and longitudinal momentum distributions and rapidity distribution of muon	28
3 Initial state QED correction	30
3.1 The scattering process $e^- + e^+ \rightarrow f + \bar{f}$	31
3.2 Initial state QED correction	32
3.2.1 Result comparison for the case of muon	34
3.2.2 Application for the cases of b-quark and c-quark	36
3.3 Higher-order QED correction	39
Conclusion and outlook	44
Bibliography	45

Introduction

Primarily, the purpose of this thesis is to provide an overview on some of the most familiar techniques of QFT to calculate several quantities of interest for a given scattering process of type $e^- + e^+ \rightarrow f + \bar{f}$ in both the theory of Quantum Electrodynamics (QED) and the Standard Model (SM). The first two chapters will be dedicated for the thorough study of $e^- + e^+ \rightarrow \mu^- + \mu^+$ in both QED and SM. Also, some comparisons will be made between the results of the two theories to help clarify the differences and similarities between them.

Indeed, the need for comparing theoretical predictions and experimental data encouraged us to proceed further and consider also soft photon emission for the respective scattering process in SM. Here, the term "soft photon" refers to real photons of low energy that could not be detected by the detectors in experiment. Since the observation of photons at low energy is not possible, the process of type $e^- + e^+ \rightarrow f + \bar{f} + n\gamma$ (where γ is a soft photon) is normally recorded as $e^- + e^+ \rightarrow f + \bar{f}$. The inclusion of photon emission effects in theoretical predictions (also known as QED correction) is, therefore, particularly important for comparison with experimental results.

In the final chapter, an overview will be provided for a better insight into QED correction and even higher-order QED correction. Moreover, the concentration will be placed on the application of QED correction in calculating two of the most crucial quantities of interest: the total cross-section and the forward-backward asymmetry. In the end, experimental results will be presented together with theoretical predictions to demonstrate that they are in better agreement when QED correction is into account.

Chapter 1

The scattering process

$e^- + e^+ \longrightarrow \mu^- + \mu^+$ in QED

1.1 An overview of QED

QED is a physics model used to describe phenomena involving electrically charged fermions, photons, and their interactions. As we know, the QED Lagrangian is:

$$\mathcal{L}_{QED} = -\frac{1}{4}F_{\mu\nu}F^{\mu\nu} - \frac{1}{2\xi}(\partial_\mu A^\mu)^2 + \bar{\psi}(i\gamma^\mu D_\mu - m)\psi. \quad (1.1.1)$$

The second rank tensor $F_{\mu\nu}$ in (1.1.1) is called the electromagnetic field tensor which is of the form:

$$F_{\mu\nu} = \partial_\mu A_\nu - \partial_\nu A_\mu, \quad (1.1.2)$$

With A_μ is a vector field. Here, we also have ψ and $\bar{\psi}$ which are correspondingly the fermion field and its adjoint. More importantly, in (1.1.1) we have used the notation of covariant derivative D_μ , which is:

$$D_\mu = \partial_\mu - ieA_\mu. \quad (1.1.3)$$

Also, ξ is real constant called the gauge fixing constant and the term with this constant is the gauge fixing term. As we can see the Lagrangian in equation (1.1.1) is a combination of three parts:

- The free electromagnetic Lagrangian with the gauge fixing term:

$$\mathcal{L}_E = -\frac{1}{4}F_{\mu\nu}F^{\mu\nu} - \frac{1}{2\xi}(\partial_\mu A^\mu)^2, \quad (1.1.4)$$

- The free fermionic Lagrangian:

$$\mathcal{L}_D = \bar{\psi}(i\gamma^\mu \partial_\mu - m)\psi, \quad (1.1.5)$$

- The interaction term, which is hidden in the covariant derivative:

$$\mathcal{L}_{int} = eA_\mu \bar{\psi}\gamma^\mu\psi. \quad (1.1.6)$$

Each part plays an essential role in the construction of QED and should be thoroughly discussed. However, we shall concentrate mostly on the free electromagnetic Lagrangian and the interaction term. Since they could help to deepen our understanding of two of the most crucial notations in QED relevant for the context of this thesis which are the general photon propagator and the vertex factor of QED.

1.1.1 The general photon propagator

By applying the principle of least action for the Lagrangian of the free electromagnetic field in (1.1.4), we shall find the equation of motion of the form:

$$\left[\square g^{\mu\rho} - \left(1 - \frac{1}{\xi}\right) \partial^\mu \partial^\rho \right] A_\rho = 0. \quad (1.1.7)$$

As we know, the propagator of the vector field $D_{\mu\nu}(x-y)$ is the solution of the inhomogeneous equation of motion (1.1.7) with a point-like source:

$$\left[\square g^{\mu\rho} - \left(1 - \frac{1}{\xi}\right) \partial^\mu \partial^\rho \right] D_{\rho\nu}(x-y) = g_\nu^\mu \delta^4(x-y). \quad (1.1.8)$$

Let's now Fourier-transform both sides of the equation (1.1.8), we shall have:

$$\left[-q^2 g^{\mu\rho} + \left(1 - \frac{1}{\xi}\right) q^\mu q^\rho \right] D_{\rho\nu}(q) = g_\nu^\mu. \quad (1.1.9)$$

Now, $D_{\rho\nu}(q)$ is actually the photon propagator that we wish to obtain. At this point, we should notice that $D_{\rho\nu}(q)$ has the form of a second rank tensor and also it must be invariant so the most general form of it should be:

$$D_{\rho\nu}(q) = A(q^2) q_\rho q_\nu + B(q^2) g_{\rho\nu}. \quad (1.1.10)$$

Inserting the general form of $D(q)$ in (1.1.10) into the equation (1.1.9), we have:

$$\begin{aligned} \Rightarrow & \left[-q^2 g^{\mu\rho} + \left(1 - \frac{1}{\xi}\right) q^\mu q^\rho \right] [A(q^2) q_\rho q_\nu + B(q^2) g_{\rho\nu}] = g_\nu^\mu \\ \Rightarrow & \begin{cases} -B(q^2) q^2 g_\nu^\mu = g_\nu^\mu \\ -A(q^2) q^2 q^\mu q_\nu + A(q^2) \left(1 - \frac{1}{\xi}\right) q^2 q^\mu q_\nu + B(q^2) \left(1 - \frac{1}{\xi}\right) q^\mu q_\nu = 0 \end{cases} \\ \Rightarrow & \begin{cases} B(q^2) = -\frac{1}{q^2} \\ A(q^2) = \frac{(1-\xi)}{q^4} \end{cases} \end{aligned} \quad (1.1.11)$$

So, the general photon propagator is of the form:

$$D_{\rho\nu}(q) = \frac{(1-\xi)}{q^4} q_\rho q_\nu - \frac{g_{\rho\nu}}{q^2}. \quad (1.1.12)$$

For ease of calculation, we normally choose ξ to be 1 (this is called the Feynman gauge). However, in next section where we discuss the Feynman amplitude which is of critical importance for the calculation of many physical quantities of interest, we shall see that the part involving the gauge fixing constant ξ does not contribute to the amplitude of a scattering process. That is to say, it is independent of ξ , and hence the choice of the gauge fixing constant could be arbitrary.

1.1.2 The vertex factor of QED

The following method of pulling out the vertex factor from the interaction term of Lagrangian was properly introduced in [1], please refer to that document for a more detailed discussion. Here, we shall apply the procedure for the case of QED for illustration. First, we have to note that the interaction term \mathcal{L}_{int} presented in the equation (1.1.6) corresponds to the Feynman diagram as in figure (1.1).

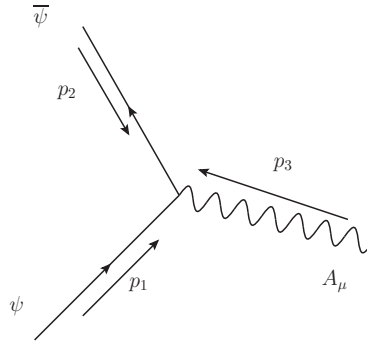


Figure 1.1: A vertex in QED

Let's now Fourier transform the three fields $\bar{\psi}$, ψ , and A_μ , we have:

$$\begin{cases} \psi(x) \longrightarrow e^{-ip_1x} \tilde{\psi}(p_1), \\ \bar{\psi}(x) \longrightarrow e^{-ip_2x} \tilde{\bar{\psi}}(p_2), \\ A_\mu(x) \longrightarrow e^{-ip_3x} \tilde{A}_\mu(p_3). \end{cases} \quad (1.1.13)$$

Inserting this into (1.1.6):

$$\mathcal{L}_{\bar{\psi}\psi A} = e \tilde{\bar{\psi}}(p_2) \gamma^\mu \tilde{\psi}(p_1) \tilde{A}_\mu(p_3) e^{-i(p_1+p_2+p_3)x} = e \tilde{\bar{\psi}}(p_2) \gamma^\mu \tilde{\psi}(p_1) \tilde{A}_\mu(p_3). \quad (1.1.14)$$

Here, the exponential factor disappears because of the conservation of momentum at the vertex, which means:

$$p_1 + p_2 + p_3 = 0. \quad (1.1.15)$$

Now, simply remove all the fields because, here, there are no identical fields. Also include the imaginary unit i and we will have the popular QED vertex factor:

$$= ie\gamma^\mu. \quad (1.1.16)$$

1.2 The Feynman amplitude

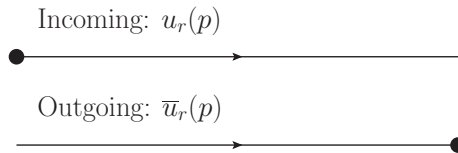
Before, we could actually write down the Feynman amplitude for the process $e^- + e^+ \longrightarrow \mu^- + \mu^+$ in QED, let's just briefly review the Feynman rules in QED, notice that here we concentrate on rules for diagrams at tree level only (for further reading, see [2]):

1. Each vertex in QED, for example the vertex μ , contributes a factor $ie\gamma^\mu$.
2. Internal lines contribute a factor as follows:

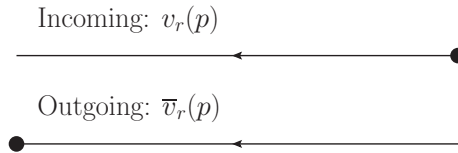
$$\left\{ \begin{array}{l} \text{Fermions: } \frac{(\not{q} + m)}{q^2 - m^2}, \text{ which is also the fermion propagator,} \\ \text{Photons: } \frac{(1 - \xi)}{q^4} q_\rho q_\nu - \frac{g_{\mu\nu}}{q^2}, \text{ which is also the general photon propagator.} \end{array} \right.$$

3. External lines contribute a factor as follows:

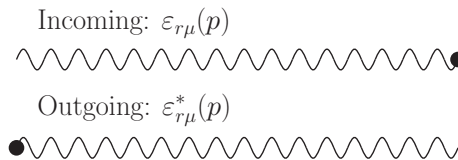
- Fermions



- Anti-fermions



- Photons



Here the indices r indicate the spin states of the spinor fields or the polarization states of the vector fields and p is the corresponding momentum of the fields.

4. The spinors are organised in a way that when we read from right to left they follow the direction of the arrows on the external lines.

5. The four-momentum of three fields at each vertex satisfy the energy-momentum conservation law.
6. If we can interchange the external lines of two incoming (or outgoing) fermions (or anti-fermions), or the external line of an incoming fermion with the one of an outgoing anti-fermion (or vice versa) of one diagram to form another diagram, we have to include a minus sign in one of the two Feynman amplitudes.

Now applying these rules for the scattering process of $e^- + e^+ \longrightarrow \mu^- + \mu^+$ in QED which has the Feynman diagram as in figure (1.2).

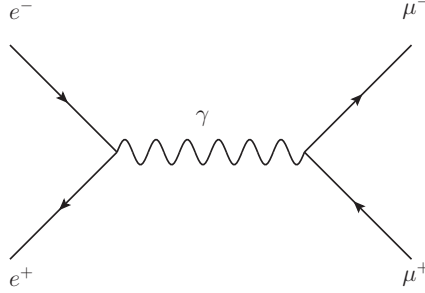


Figure 1.2: The Feynman diagram of $e^- + e^+ \longrightarrow \mu^- + \mu^+$ in QED

Let's denote the four momenta and spin indices of e^- , e^+ , μ^- , and μ^+ to be (p, s) , (p', s') , (k, r) , and (p', r') correspondingly. From the diagram in figure (1.2), we can write the Feynman amplitude for this process as follow:

$$\begin{aligned}
 \mathcal{M} &= [\bar{v}_{s'}(p')(ie\gamma^\mu)u_s(p)] \left[\frac{(1-\xi)q_\mu q_\nu}{q^4} - \frac{g_{\mu\nu}}{q^2} \right] [\bar{u}_r(k)(ie\gamma^\nu)v_{r'}(k')] \\
 &= -\frac{(1-\xi)e^2}{q^4} [\bar{v}_{s'}(p')\not{q}u_s(p)][\bar{u}_r(k)\not{q}v_{r'}(k')] + \frac{e^2}{q^2} [\bar{v}_{s'}(p')\gamma^\mu u_s(p)][\bar{u}_r(k)\gamma_\mu v_{r'}(k')].
 \end{aligned} \tag{1.2.1}$$

Let's now focus on the term $[\bar{v}_{s'}(p')\not{q}u_s(p)]$:

$$\bar{v}_{s'}(p')\not{q}u_s(p) = \bar{v}_{s'}(p')(\not{p} + \not{p}')u_s(p) = m_e\bar{v}_{s'}(p')u_s(p) - m_e\bar{v}_{s'}(p')u_s(p) = 0. \tag{1.2.2}$$

In the calculation above, we have exploited the law of momentum conservation at the vertex, which could be written as $q = p + p'$. We also used these two identities:

$$\begin{cases} \not{p}u_s(p) = m_e u_s(p), \\ \bar{v}_{s'}(p')\not{p}' = -m_e\bar{v}_{s'}(p'). \end{cases} \tag{1.2.3}$$

From (1.2.2) we can see that \mathcal{M} does not depend on ξ as being stressed before. At this point, we shall have:

$$\mathcal{M} = \frac{e^2}{q^2} [\bar{v}_{s'}(p')\gamma^\mu u_s(p)][\bar{u}_r(k)\gamma_\mu v_{r'}(k')]. \tag{1.2.4}$$

Now, we are in position to write down the squared amplitude:

$$|\mathcal{M}|^2 = \mathcal{M}^\dagger \mathcal{M} = \frac{e^4}{q^4} [\bar{v}_{s'}(p')\gamma^\nu u_s(p)][\bar{u}_s(p)\gamma^\mu v_{s'}(p')][\bar{v}_{r'}(k')\gamma_\mu u_r(k)][\bar{u}_r(k)\gamma_\nu v_{r'}(k')]. \tag{1.2.5}$$

Besides, we have to notice that if we ignore the spin states of both the incoming and outgoing beams, we have to average the square of the amplitude $|\mathcal{M}|^2$ in (1.2.5) on initial spin indices and sum over subsequent spin indices. Thus, the squared amplitude is:

$$|\mathcal{M}_0|^2 = \frac{1}{4} \sum_{s,s',r,r'} \mathcal{M} \mathcal{M}^\dagger = \frac{e^4}{4q^4} \text{Tr}((\not{p}' - m_e)\gamma^\mu(\not{p} + m_e)\gamma^\nu) \text{Tr}((\not{k}' - m_\mu)\gamma_\mu(\not{k} + m_\mu)\gamma_\nu). \quad (1.2.6)$$

Notice that to actually derive the formula (1.2.6), we have used:

$$\begin{cases} \sum_s u_s(p)\bar{u}_s(p) = \not{p} + m_e, \\ \sum_{s'} v_{s'}(p')\bar{v}_{s'}(p') = \not{p}' - m_e, \\ \sum_r u_r(k)\bar{u}_r(k) = \not{k} + m_\mu, \\ \sum_{r'} v_{r'}(k)\bar{v}_{r'}(k) = \not{k}' - m_\mu. \end{cases} \quad (1.2.7)$$

We should also notice these identities for ease of calculation:

$$\text{Tr}(\gamma^\sigma \gamma^\mu \gamma^\lambda \gamma^\nu) = 4(g^{\sigma\mu}g^{\lambda\nu} - g^{\sigma\lambda}g^{\mu\nu} + g^{\sigma\nu}g^{\mu\lambda}), \quad (1.2.8)$$

$$\text{Tr}(\gamma^\mu \gamma^\nu) = 4g^{\mu\nu}. \quad (1.2.9)$$

Similarly, we have:

$$\text{Tr}(\gamma_\sigma \gamma_\mu \gamma_\lambda \gamma_\nu) = 4(g_{\sigma\mu}g_{\lambda\nu} - g_{\sigma\lambda}g_{\mu\nu} + g_{\sigma\nu}g_{\mu\lambda}), \quad (1.2.10)$$

$$\text{Tr}(\gamma_\mu \gamma_\nu) = 4g_{\mu\nu}. \quad (1.2.11)$$

Applying the identities above, we will be able to obtain the results for the two traces in (1.2.6) as follow:

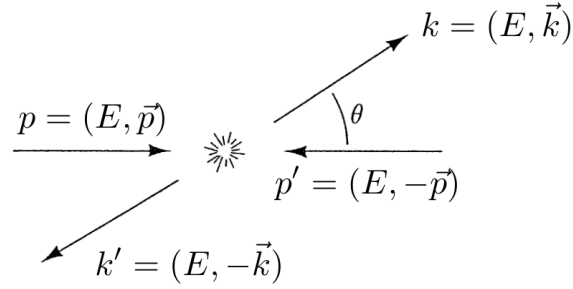
$$\begin{cases} \text{Tr}((\not{p}' - m_e)\gamma^\mu(\not{p} + m_e)\gamma^\nu) = 4(p^\mu p'^\nu - p p' g^{\mu\nu} + p^\nu p'^\mu - m_e^2 g^{\mu\nu}), \\ \text{Tr}((\not{k}' - m_\mu)\gamma_\mu(\not{k} + m_\mu)\gamma_\nu) = 4(k'_\mu k_\nu - k' k g_{\mu\nu} + k'_\nu k_\mu - m_\mu^2 g_{\mu\nu}). \end{cases} \quad (1.2.12)$$

We now insert (1.2.12) in (1.2.6):

$$|\mathcal{M}_0|^2 = \frac{8e^4}{q^4} [(p \cdot k')(p' \cdot k) + (p' \cdot k')(p \cdot k) + m_\mu^2(p \cdot p') + m_e^2(k \cdot k') + 2m_e^2 m_\mu^2]. \quad (1.2.13)$$

Then, let's choose to work specifically in CM frame. Also we have to assign the energy and momentum of each particles in the process as drawn in figure (1.3). Now, in order to further proceed with the calculation using of $|\mathcal{M}_0|^2$, it is better to make an approximation. From now on, we shall set $m_e = 0$ (this approximation is appropriate in this case because $m_\mu \gg m_e$), we, therefore, have $|\vec{p}|^2 = E^2$. That leads to several kinematic relations as presented below:

$$\Rightarrow \begin{cases} p \cdot k = p' \cdot k' = E^2 - \vec{p} \cdot \vec{k} = E^2 - E|\vec{k}| \cos \theta \\ p \cdot k' = p' \cdot k = E^2 + \vec{p} \cdot \vec{k} = E^2 + E|\vec{k}| \cos \theta \\ q^2 = (p + p')^2 = 4E^2 \\ p \cdot p' = 2E^2 \\ k \cdot k' = E^2 + |\vec{k}|^2 \end{cases} \quad (1.2.14)$$


 Figure 1.3: The scattering process $e^- + e^+ \longrightarrow \mu^- + \mu^+$ in CM frame

Inserting relations in (1.2.14) into (1.2.13), we shall have:

$$|\mathcal{M}_0|^2 = \frac{e^4}{E^2} \left[(E^2 + m_\mu^2) + (E^2 - m_\mu^2) \cos^2 \theta \right].$$

1.3 Several physical quantities of interest

1.3.1 The differential cross-section and the total cross-section

For scattering process $e^- + e^+ \longrightarrow \mu^- + \mu^+$, we have the differential cross section to be of the form:

$$\frac{d\sigma}{d\Omega} = \frac{1}{64\pi^2} \frac{|\mathcal{M}_0|^2}{(E_{e^-} + E_{e^+})^2 |\vec{p}|} = \frac{|\vec{k}|e^4}{256\pi^2 E^5} \left[(E^2 + m_\mu^2) + (E^2 - m_\mu^2) \cos^2 \theta \right], \quad (1.3.1)$$

Physically speaking, the differential cross-section would allow us to find the probability that μ^- (or μ^+) would have the spatial momentum \vec{k} (or $-\vec{k}$) in the direction with angular coordinate (θ, φ) after pair creation. Now, in order to deduce the total cross-section, we could simply integrate the differential cross-section over every directions in space. We have:

$$\begin{aligned} \sigma_T = \int \frac{d\sigma}{d\Omega} d\Omega &\Rightarrow \sigma_T = \frac{|\vec{k}|e^4}{256\pi^2 E^5} \int \left[(E^2 + m_\mu^2) + (E^2 - m_\mu^2) \cos^2 \theta \right] d\Omega \\ &= \frac{|\vec{k}|e^4}{48\pi E^5} \left(E^2 + \frac{1}{2}m_\mu^2 \right) \end{aligned} \quad (1.3.2)$$

This total cross-section would allow us to know on average the total number of muons that are generated after the annihilation of a pair of electron and positron. It is because number of muons N_μ is proportional to σ with the factor of proportionality to be L -the luminosity of the beam of incident particles.

The figure (1.4) illustrates the dependence of the total cross-section on $\sqrt{s} = 2E$ which is the total energy of the scattering process in CM frame. We could see that the total cross-section graph begins at the total energy of about $\sqrt{s} = 2m_\mu \simeq 0.21$ GeV. This feature is what we have expected, since the threshold energy for pair creation must be two times of the mass of muon.

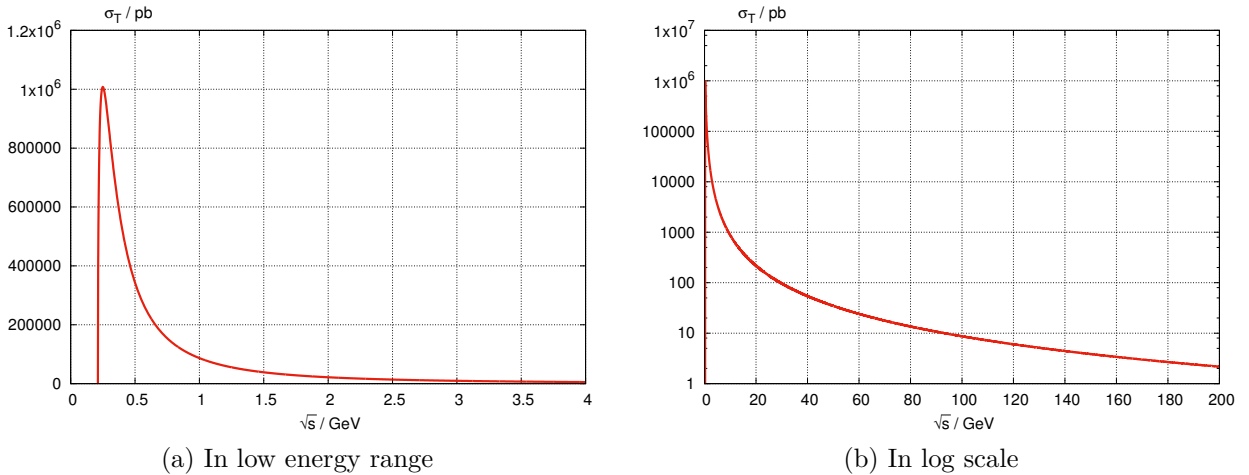


Figure 1.4: Total cross-section of muon

1.3.2 Angular distribution of muon

The angular distribution of muon is of critical importance, since it allows us to seek for direction with high probability of getting muon. This distribution is nothing but the integration of the differential cross-section with regards to φ , we have:

$$\begin{aligned} \frac{d\sigma}{d\theta} &= \int_0^{2\pi} \frac{|\vec{k}|e^4}{256\pi^2 E^5} \left[(E^2 + m_\mu^2) + (E^2 - m_\mu^2) \cos^2 \theta \right] \sin \theta d\varphi \\ &= \frac{|\vec{k}|e^4}{128\pi E^5} \left[(E^2 + m_\mu^2) + (E^2 - m_\mu^2) \cos^2 \theta \right] \sin \theta. \end{aligned} \quad (1.3.3)$$

Figure (1.5) shows the angular distribution of muon in the case that CM energy of electron is 10 GeV. As could be seen, there are two peaks in this distribution corresponding to $\theta \simeq 0.95$ rad and $\theta \simeq 2.19$ rad. That means if we are looking for muon of this scattering event in the range of total energy at about 20 GeV, it is more sensible to look for detectors in those angles.

Besides, we could see that this distribution is essentially zero at $\theta = 0$ and $\theta = \pi$. This means that there is no event of pair creation in which muon has velocity parallel to the electron beam axis.

1.3.3 Transverse momentum and longitudinal momentum distributions of muon

Another quantity of interest is the transverse momentum distribution of muons after pair creation. The distribution should be a function of k_t -the transverse momentum and to deduce the analytical form of this distribution means to find $d\sigma/dk_t$. Our task now is simply to switch from angular distribution to momentum distribution. In general, if we want to switch from distribution $p(x)$ to $p_F(f)$ with $f = F(x)$, we could simply use the following formula:

$$p_F(f) = \sum_i p(x_i) \mathcal{J}_i = \sum_i p(x_i) \left. \frac{dx}{dF} \right|_{x=x_i}. \quad (1.3.4)$$

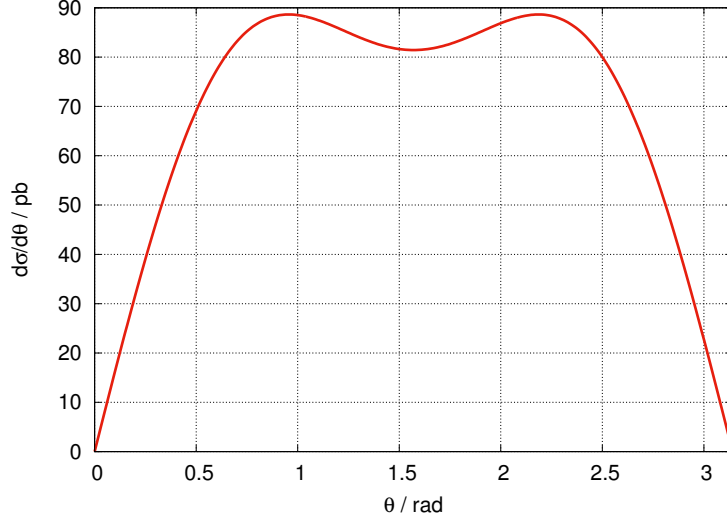


Figure 1.5: Angular distribution of muon with $\sqrt{s} = 20$ GeV

The factor \mathcal{J}_i is called the Jacobians associated with the change of variables from x to F (further discussion could be found in [3]). Now, for the transverse momentum, we have:

$$k_t = |\vec{k}| \sin \theta \Rightarrow \begin{cases} \theta_1 = \arcsin \frac{k_t}{|\vec{k}|} \\ \theta_2 = \pi - \arcsin \frac{k_t}{|\vec{k}|} \end{cases} \quad (1.3.5)$$

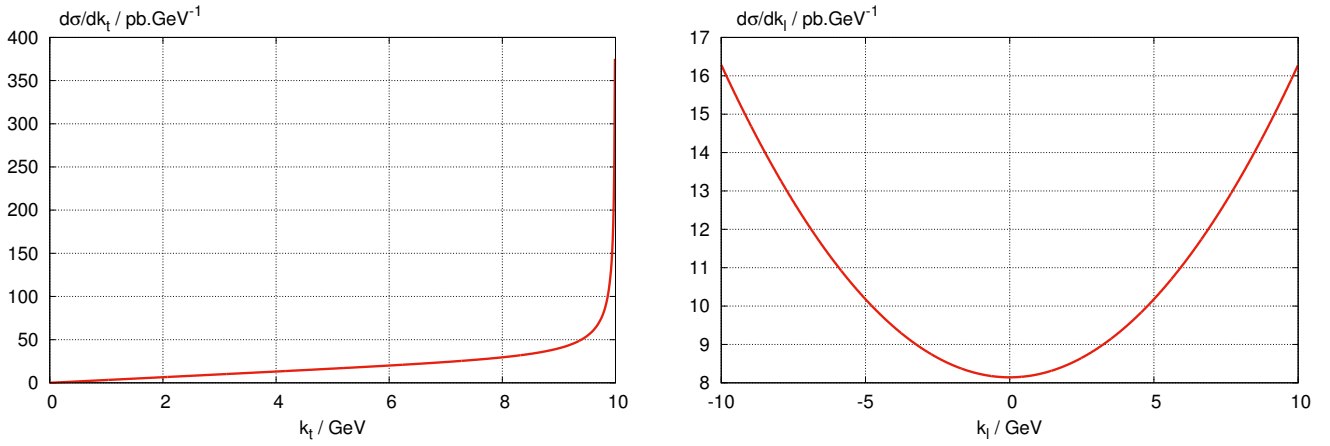
Also, we have the Jacobians are:

$$\left| \frac{d\theta}{dk_t} \right| = \frac{1}{|\vec{k}| |\cos \theta|} \Rightarrow \left| \frac{d\theta}{dk_t} \right|_{\theta=\theta_1} = \left| \frac{d\theta}{dk_t} \right|_{\theta=\theta_2} = \frac{1}{\sqrt{|\vec{k}|^2 - k_t^2}} \quad (1.3.6)$$

Now, we shall use the formula (1.3.4) presented above:

$$\frac{d\sigma}{dk_t} = \sum_i \frac{d\sigma}{d\theta} \bigg|_{\theta=\theta_i} \left| \frac{d\theta}{dk_t} \right|_{\theta=\theta_i} \Rightarrow \frac{d\sigma}{dk_t} = \frac{k_t (2E^2 - k_t^2) e^4}{64\pi E^5 \sqrt{|\vec{k}|^2 - k_t^2}}. \quad (1.3.7)$$

With the formula (1.3.7), we are able to plot the transverse momentum distribution of muon with CM energy of about 10 GeV (figure (1.6a)) for illustration.



(a) Transverse momentum distribution of muon

(b) Longitudinal momentum distribution

Figure 1.6: Transverse and longitudinal momentum distributions with $\sqrt{s} = 20$ GeV

In the same manner, we could find the longitudinal momentum distribution of muon, for the longitudinal momentum we have:

$$k_l = |\vec{k}| \cos \theta \Rightarrow \begin{cases} \theta_1 = \arccos \frac{k_l}{|\vec{k}|} \\ \theta_2 = -\arccos \frac{k_l}{|\vec{k}|} \end{cases} \quad (1.3.8)$$

We only take the solution θ_1 since $\theta \in [0; \pi]$. The associated Jacobian is:

$$\left| \frac{d\theta}{dk_l} \right| = \frac{1}{|\vec{k}| |\sin \theta|} \Rightarrow \left| \frac{d\theta}{dk_l} \right|_{\theta=\theta_1} = \frac{1}{\sqrt{|\vec{k}|^2 - k_l^2}}. \quad (1.3.9)$$

Now, to switch from θ distribution to k_l distribution, we have:

$$\frac{d\sigma}{dk_l} = \frac{d\sigma}{d\theta} \left| \frac{d\theta}{dk_l} \right|_{\theta=\theta_1} = \frac{e^4}{128\pi E^5} (E^2 + m_\mu^2 + k_l^2) \quad (1.3.10)$$

Figure (1.6b) depicts the graph of the longitudinal momentum distribution of muon with CM energy of about 10 GeV.

1.3.4 Rapidity and pseudo-rapidity distributions of muon

Let's first discuss the necessity of rapidity distribution. Basically, rapidity is defined as:

$$y = \frac{1}{2} \ln \left(\frac{E + k_l}{E - k_l} \right). \quad (1.3.11)$$

From this definition we can see that if $k_l \rightarrow \pm E$, i.e. $\vec{k} \parallel Oz$ (notice that here we assigned Oz to be the direction of the electron beam), the rapidity, in this case, goes to infinity meaning $y \rightarrow \pm\infty$. On the other hand, if $\vec{k} \perp Oz$, we, then, have $y \rightarrow 0$ since

$k_l = 0$. From that we could see that there should be a relation between the outgoing angle $\theta = (\vec{k}, Oz)$ and the rapidity of a particle. Hence, rapidity is often paired with the azimuthal coordinate φ as a spatial coordinate for particles analysis in accelerator physics. For simplicity, we shall present another way to write the rapidity of a particle that is exactly equivalent to the original definition:

$$y = \operatorname{arctanh} \frac{k_l}{E}. \quad (1.3.12)$$

This would allow us to find the rapidity distribution from the longitudinal distribution deduced in equation (1.3.10). We could simply repeat the procedure of changing variable. From (1.3.12) we could see that:

$$k_l = E \tanh y \Rightarrow \left. \frac{dk_l}{dy} \right|_{k_l = E \tanh y} = E(1 - \tanh^2 y) \quad (1.3.13)$$

From the longitudinal momentum distribution in (1.3.10) and the formula (1.3.4), we have:

$$\frac{d\sigma}{dy} = \left. \frac{d\sigma}{dk_l} \right|_{k_l = E \tanh y} \left. \frac{dk_l}{dy} \right|_{k_l = E \tanh y} = \frac{e^4}{128\pi E^4 \cosh^2 y} [m_\mu^2 + E^2(1 + \tanh^2 y)]. \quad (1.3.14)$$

A plot of rapidity distribution of muon with energy in CM frame of about 10 GeV is presented in figure (1.7a).

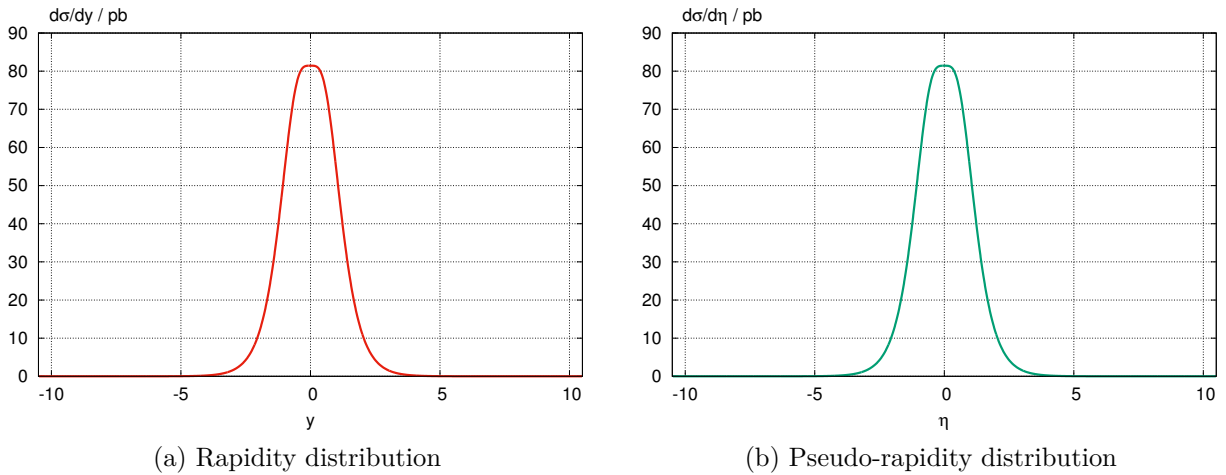


Figure 1.7: Rapidity and pseudo-rapidity distribution for $\sqrt{s} = 20$ GeV

Besides, accelerator physicists also use another quantity that is actually not much different from rapidity for ultra-relativistic particles. It is called pseudo-rapidity and it is defined as:

$$\eta = \frac{1}{2} \ln \left(\frac{|\vec{k}| + k_l}{|\vec{k}| - k_l} \right) \quad (1.3.15)$$

It is not quite hard to prove that for ultra-relativistic particles, which have very large energy compared to its mass, rapidity is approximately equal to pseudo-rapidity. In addition, we could also express pseudo-rapidity as a function of θ :

$$\eta = -\ln\left(\tan\frac{\theta}{2}\right). \quad (1.3.16)$$

Since measurement of θ could be done quite straightforward, the distribution of pseudo-rapidity might be easier to be obtained in experiment. Now, we shall deduce the pseudo-rapidity distribution theoretically. Because of the relation between pseudo-rapidity and polar angle, we would rather choose to deduce the distribution of pseudo-rapidity from the angular distribution. From the formula of pseudo-rapidity in (1.3.16), we have:

$$\theta = 2 \arctan(e^{-\eta}) \quad (1.3.17)$$

Also, it is clearer to explicitly point out several identities related to η and θ :

$$\tan\frac{\theta}{2} = e^{-\eta} \Rightarrow \begin{cases} \sin\theta = \frac{1}{\cosh\eta} \\ \cos^2\theta = 1 - \sin^2\theta = \tanh^2\eta \end{cases} \quad (1.3.18)$$

The corresponding Jacobian for changing variable is:

$$\left|\frac{d\theta}{d\eta}\right|_{\theta=2\arctan(e^{-\eta})} = \left|\frac{-2e^{-\eta}}{1+e^{-2\eta}}\right| = \left|\frac{-2}{e^\eta+e^{-\eta}}\right| = \frac{1}{\cosh\eta}. \quad (1.3.19)$$

Once again we will use the usual technique of changing variable to deduce the pseudo-rapidity distribution. From (1.3.3), (1.3.18), and (1.3.19), we have:

$$\begin{aligned} \frac{d\sigma}{d\eta} &= \frac{d\sigma}{d\theta} \Big|_{\theta=2\arctan(e^{-\eta})} \left| \frac{d\theta}{d\eta} \right|_{\theta=2\arctan(e^{-\eta})} \\ \Rightarrow \frac{d\sigma}{d\eta} &= \frac{|\vec{k}|e^4}{128\pi E^5 \cosh^2\eta} \left[(E^2 + m_\mu^2) + (E^2 - m_\mu^2) \tanh^2\eta \right]. \end{aligned} \quad (1.3.20)$$

From this result we could see that if muon has relatively high energy which means $E^2 - m_\mu^2 \simeq E^2$, then the pseudo-rapidity distribution will be approximately equal to the rapidity distribution. For illustration, the plot of the pseudo-rapidity distribution of muon with CM energy of about 10 GeV is presented in figure (1.7b). As we can see, the two plots are exactly the same since m_μ is quite small compared to E , the two peaks at $y = \eta = 0$.

Chapter 2

The scattering process

$$e^- + e^+ \longrightarrow \mu^- + \mu^+ \text{ in SM}$$

2.1 An overview of SM

SM is a physics model dealing with elementary particles using QFT and group theory as a mathematical framework. In SM, there are three generations of elementary particles which are presented in the table (2.1).

First Generation	Second Generation	Third Generation
Leptons		
ν_e e	ν_μ μ	ν_τ τ
Quarks		
u d	c s	t b

Table 2.1: Elementary particles

SM allows us to describe a wide range phenomena relating to those elementary particles. Essentially, particle physicists consider only strong and electroweak interactions between elementary particles (gravitational interactions has not yet been included in SM). Those interactions are mediated by gauge vector bosons which are photon, Z -boson, and W -boson for electroweak interaction and gluon for strong interaction. As we know, the Lagrangian of SM is of the form:

$$\mathcal{L} = \mathcal{L}_{fermion} + \mathcal{L}_{gauge} + \mathcal{L}_{Higgs} + \mathcal{L}_{Yukawa} + \mathcal{L}_{gf} + \mathcal{L}_{ghost} \quad (2.1.1)$$

Indeed, the first two term ($\mathcal{L}_{fermion}$ and \mathcal{L}_{gauge}) in (2.1.1) will be studied further in the following subsections. The other terms which are the Higgs term (\mathcal{L}_{Higgs}), the Yukawa term (\mathcal{L}_{Yukawa}), the gauge fixing (\mathcal{L}_{gf}), and the Fadeev-Popov ghost term (\mathcal{L}_{ghost}) might be omitted from our discussion since they are not quite relevant in the context of this thesis. At this moment, the most essential point to note is that the SM Lagrangian is set to be invariant under the transformation of the group $SU(3)_C \otimes SU(2)_L \otimes U(1)_Y$. However, the concentration of this thesis will be on the behaviour of particles around the

range of Z -peak (\sqrt{s} is around $m_Z \simeq 91$ GeV) when we consider also effects of soft photon emission, we shall confine ourselves mainly to $SU(2)_L \otimes U(1)_Y$. Another thing to point out is that in this model, left-handed and right-handed fields transform differently, since we organise left-handed fields into doublet and right-handed ones into singlet. Notice that only doublets are affected by element of $SU(2)_L$ which means:

$$\begin{cases} L \longrightarrow L' = \exp \left\{ ig \frac{\sigma^i}{2} \alpha_i(x) \right\} L \\ R \longrightarrow R' = R \end{cases} \quad (2.1.2)$$

Where σ^i are three Pauli matrices and they are also generators of $SU(2)_L$. As for the group $U(1)_Y$, the transformations are:

$$\begin{cases} L \longrightarrow L' = \exp \left\{ ig' \frac{Y}{2} \beta(x) \right\} L \\ R \longrightarrow R' = \exp \left\{ ig' \frac{Y}{2} \beta(x) \right\} R \end{cases} \quad (2.1.3)$$

In the law of transformation above, we have introduced the weak hypercharge Y . It is also important to note that the values of Y are different for different particles. The weak hypercharges of each elementary particles could be evaluated by Gell-Mann–Nishijima formula, that is:

$$Q = I^3 + \frac{Y}{2}. \quad (2.1.4)$$

With Q is the charge of the particle and I^3 is the isospin defined as eigenvalue of $\sigma^3/2$ for doublets and $I^3 = 0$ for singlets.

Before proceeding further, we should notice that from now on the fields will be denoted by the symbols of the corresponding particles. For example, left-handed and right-handed fermionic fields of electrons will be represented by e_L and e_R respectively.

2.1.1 The fermionic term of SM Lagrangian

The first term of the SM Lagrangian in equation (2.1.1) is:

$$\mathcal{L}_{fermion} = \sum_f i \bar{L}_f \not{D} L_f + i \bar{R}_f \not{D} R_f. \quad (2.1.5)$$

The sum is taken over all species of fermions in the SM. Now, notice that in equation (2.1.5), we also used the covariant derivative. However, for the left-handed and right-handed fermionic fields, the covariant derivatives are different due to their distinct laws of transformation under $SU(2)_L \otimes U(1)_Y$ presented in equation (2.1.2). We have:

$$\begin{cases} D_\mu L_f = \left(\partial_\mu - ig \frac{\sigma^i}{2} W_\mu^a - ig' \frac{Y}{2} B_\mu \right) L_f \\ D_\mu R_f = \left(\partial_\mu - ig' \frac{Y}{2} B_\mu \right) R_f \end{cases} \quad (2.1.6)$$

Here, W_μ^a ($a = \overline{1, 3}$) are the three gauge fields of $SU(2)_L$ and B_μ is the corresponding gauge field of $U(1)_Y$. We can probably see that it is quite similar to the case of QED, by inserting (2.1.6) into (2.1.5) we could deduce several terms that look like interaction terms of the fermionic fields with the gauge fields. Nevertheless, it is crucial to note that the gauge fields introduced here are not physical fields, but rather their linear combinations are. The physical fields could be written as:

$$\begin{cases} W_\mu^\pm = \frac{1}{\sqrt{2}}(W_\mu^1 \mp iW_\mu^2) \\ Z_\mu = W_\mu^3 c_W + B_\mu s_W \\ A_\mu = -W_\mu^3 s_W + B_\mu c_W \end{cases} \quad (2.1.7)$$

Here, we have $c_W = \cos \theta_W$ and $s_W = \sin \theta_W$, where θ_W is the famous weak mixing angle defined as $\theta_W = \arctan(g'/g)$ ¹. In fact, a more thorough study of the Higgs term of SM Lagrangian will reveal that by applying the linear combinations in (2.1.7) we will be able to find the masses of Z -boson, W -boson, and photon (represented by Z_μ , W_μ^\pm , and A_μ respectively).

2.1.2 The gauge fields in SM

The next term to be analysed in the SM Lagrangian is the gauge field Lagrangian. It is of the form:

$$\mathcal{L}_{gauge} = -\frac{1}{4}F_{\mu\nu}F^{\mu\nu} - \frac{1}{4}W_{\mu\nu}^a W^{a\mu\nu}. \quad (2.1.8)$$

In equation (2.1.8), $W_{\mu\nu}^a$ and $F_{\mu\nu}$ are called the field tensors corresponding to the gauge fields of $SU(2)_L$ and $U(1)_Y$ respectively. Their explicit form could be written as:

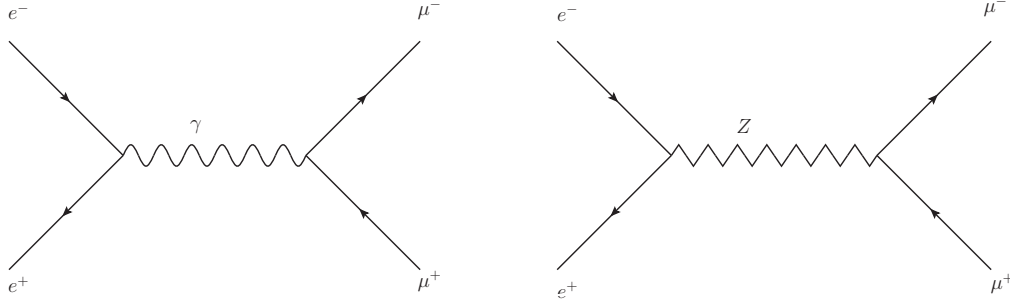
$$\begin{cases} W_{\mu\nu}^a = \partial_\mu W_\nu^a - \partial_\nu W_\mu^a + g\epsilon_{abc}W_\mu^b W_\nu^c \\ F_{\mu\nu} = \partial_\mu B_\nu - \partial_\nu B_\mu \end{cases} \quad (2.1.9)$$

We could see that for the non-Abelian group $SU(2)_L$, there is a term containing the structure constant which appears in the field tensor. In the case of the group $SU(2)_L$, the structure constant is nothing but the familiar Levi-Civita tensor.

2.2 The vertex factor of Z -boson

In this chapter, we will try to re-deduce all the distributions as in the first chapter but more precisely by applying SM. Here, we shall consider only two diagrams (presented in figure (2.1)) for muon pair creation in the scattering process of e^- and e^+ . In fact, there are more than just two mediators for such process meaning more diagrams should be considered for more precise calculation. However, the contribution of such diagrams are relatively small and hence could be ignored.

¹In this thesis, if not indicated, we will take $c_W = m_W/m_Z$. Here, m_W and m_Z are correspondingly W -boson and Z -boson mass from experiment ($m_W \simeq 80.385$ GeV and $m_Z \simeq 91.1876$ GeV).


 Figure 2.1: The Feynman diagrams of $e^- + e^+ \longrightarrow \mu^- + \mu^+$ in SM

Regarding the process mediating by photon, it is nothing but the same process that was closely studied in the first chapter. Hence, we could re-use the result of the amplitude deduced in equation (1.2.4). Nevertheless, the second diagram involves Z -boson as a mediator. Thus, the vertex factor and also the propagator for that case have to be derived.

2.2.1 The neutral part of the covariant derivative

First, we have to notice that the weak interaction of both left-handed and right-handed fermions mediating by Z boson only appears in the kinetic term of the fermionic Lagrangian in (2.1.5). Also, we should note that to see the coupling constants of fermions in weak interaction mediated by Z bosons, we have to seek for the part of the covariant derivative that contains Z_μ . However, Z_μ does not appear explicitly in (2.1.6), it is rather a linear combination of W_μ^3 and B_μ . We shall, therefore, work with the part that involves the gauge fields W_μ^3 and B_μ only. Let's call it D_μ^N which corresponds to the weak interaction mediated by neutral particles like Z bosons or photons. We have:

$$\begin{cases} D_\mu^N L_f = \left(-ig \frac{\sigma^3}{2} W_\mu^3 - ig' \frac{Y}{2} B_\mu \right) L_f \\ D_\mu^N R_f = \left(-ig' \frac{Y}{2} B_\mu \right) R_f \end{cases} \quad (2.2.1)$$

From (2.1.7), we could deduce the inverse transformation:

$$\begin{cases} W_\mu^3 = c_W Z_\mu + s_W A_\mu \\ B_\mu = -s_W Z_\mu + c_W A_\mu \end{cases} \quad (2.2.2)$$

Now, inserting (2.2.2) into (2.2.1), we have:

$$\begin{cases} D_\mu^N L_f = \left[-\frac{ig}{c_W} \left(c_W^2 \frac{\sigma^3}{2} - s_W^2 \frac{Y}{2} \right) Z_\mu - igs_W \left(\frac{\sigma^3}{2} + \frac{Y}{2} \right) A_\mu \right] L_f \\ D_\mu^N R_f = \left(\frac{ig}{c_W} s_W^2 \frac{Y}{2} Z_\mu - \frac{ig}{c_W} s_W c_W \frac{Y}{2} A_\mu \right) R_f \end{cases} \quad (2.2.3)$$

2.2.2 Left-handed electrons

Let's first focus on the the left-handed term of the neutral part of the covariant derivative:

$$D_\mu^N L_f = \left[-\frac{ig}{c_W} \left(c_W^2 \frac{\sigma^3}{2} - s_W^2 \frac{Y}{2} \right) Z_\mu - igs_W \left(\frac{\sigma^3}{2} + \frac{Y}{2} \right) A_\mu \right] L_f. \quad (2.2.4)$$

Now, we shall first concentrate on the doublet of left-handed ν_e and e , the corresponding Lagrangian could be written as:

$$\begin{aligned}
 \bar{L}_e \gamma^\mu D_\mu^N L_e &= i (\bar{\nu}_e \ \bar{e})_L \gamma^\mu \left[-\frac{ig}{c_W} \left(c_W^2 \frac{\sigma^3}{2} - s_W^2 \frac{Y}{2} \right) Z_\mu - ig_{SW} \left(\frac{\sigma^3}{2} + \frac{Y}{2} \right) A_\mu \right] \begin{pmatrix} \nu_e \\ e \end{pmatrix}_L \\
 &= i \bar{\nu}_{eL} \gamma^\mu \left[-\frac{ig}{c_W} \left(c_W^2 \frac{\sigma^3}{2} - s_W^2 \frac{Y}{2} \right) Z_\mu - ig_{SW} \left(\frac{\sigma^3}{2} + \frac{Y}{2} \right) A_\mu \right] \nu_{eL} \\
 &\quad + i \bar{e}_L \gamma^\mu \left[-\frac{ig}{c_W} \left(c_W^2 \frac{\sigma^3}{2} - s_W^2 \frac{Y}{2} \right) Z_\mu - ig_{SW} \left(\frac{\sigma^3}{2} + \frac{Y}{2} \right) A_\mu \right] e_L
 \end{aligned} \tag{2.2.5}$$

Besides, we should bear in mind that:

$$\begin{cases} \frac{\sigma^3}{2} \nu_{eL} = I_\nu^3 \nu_{eL} = \frac{1}{2} \nu_{eL} \\ \frac{\sigma^3}{2} e_L = I_e^3 e_L = -\frac{1}{2} e_L \end{cases} \tag{2.2.6}$$

Inserting (2.2.6) into (2.2.5), we have:

$$\begin{aligned}
 i \bar{L}_e \gamma^\mu D_\mu^N L_e &= \frac{g}{c_W} \left(c_W^2 I_\nu^3 - s_W^2 \frac{Y}{2} \right) Z_\mu (\bar{\nu}_{eL} \gamma^\mu \nu_{eL}) + g_{SW} Q_\nu A_\mu (\bar{\nu}_{eL} \gamma^\mu \nu_{eL}) \\
 &\quad + \frac{g}{c_W} \left(c_W^2 I_e^3 - s_W^2 \frac{Y}{2} \right) Z_\mu (\bar{e}_L \gamma^\mu e_L) + g_{SW} Q_e A_\mu (\bar{e}_L \gamma^\mu e_L)
 \end{aligned} \tag{2.2.7}$$

In the first term of (2.2.5), we can see the coupling constant of left-handed e in weak interaction mediated by Z bosons is:

$$g_L = \frac{g}{c_W} \left(c_W^2 I_e^3 - s_W^2 \frac{Y}{2} \right) = \frac{g}{c_W} \left(-\frac{1}{2} + s_W^2 \right). \tag{2.2.8}$$

In (2.2.8), we have inserted the numerical values of weak isospin of left-handed electron which is $I_e^3 = -1/2$ and the weak hypercharge of left-handed doublet of ν_e and e which is $Y = -1$.

2.2.3 Right-handed electrons

For the right-handed electron. As could be seen from (2.2.3), the corresponding Lagrangian is written as:

$$\begin{aligned}
 i \bar{e}_R \gamma^\mu D_\mu^N e_R &= i \bar{e}_R \gamma^\mu \left(\frac{ig}{c_W} s_W^2 \frac{Y}{2} Z_\mu - \frac{ig}{c_W} s_W c_W \frac{Y}{2} A_\mu \right) e_R \\
 &= -\frac{g}{c_W} s_W^2 \frac{Y}{2} Z_\mu (\bar{e}_R \gamma^\mu e_R) + \frac{g}{c_W} s_W c_W \frac{Y}{2} A_\mu (\bar{e}_R \gamma^\mu e_R).
 \end{aligned} \tag{2.2.9}$$

From (2.2.9), we could pull out the coupling constant of right-handed electron in weak interaction mediated by Z bosons, which is as the following:

$$g_R = -\frac{g}{c_W} s_W^2 \frac{Y}{2} = \frac{g}{c_W} s_W^2 \tag{2.2.10}$$

Again in (2.2.10), we have used the numerical value of the weak hypercharge in the case of right-handed electrons $Y = -2$ (because $I_e^3 = 0$ for right-handed electrons).

2.2.4 The vertex factor of eeZ

Now, as we have proven in the last two sections (see the first terms of equation (2.2.7) and (2.2.9)), the interaction term of e^- and e^+ mediated by Z boson could be written as:

$$\mathcal{L}_{int}^{\bar{e}eZ} = g_L Z_\mu (\bar{e}_L \gamma^\mu e_L) + g_R Z_\mu (\bar{e}_R \gamma^\mu e_R). \quad (2.2.11)$$

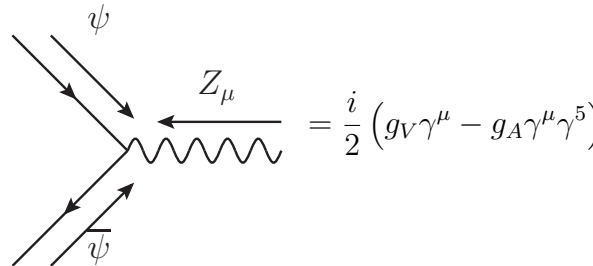
If we want to find the vertex factor, we should be able to re-write the current in terms of the fields \bar{e} and e . In order to do so, we should notice that:

$$\begin{cases} e_L = \frac{1 - \gamma^5}{2} e \\ e_R = \frac{1 + \gamma^5}{2} e \end{cases} \quad (2.2.12)$$

Inserting the identities in (2.2.12) into (2.2.11), we will have:

$$\mathcal{L}_{int}^{\bar{e}eZ} = \frac{1}{2} Z_\mu \left[(g_L + g_R) (\bar{e} \gamma^\mu e) - (g_L - g_R) (\bar{e} \gamma^\mu \gamma^5 e) \right] = Z_\mu \left[g_V (\bar{e} \gamma^\mu e) - g_A (\bar{e} \gamma^\mu \gamma^5 e) \right] \quad (2.2.13)$$

With g_L and g_R deduced in (2.2.10) and (2.2.8), the coupling constants g_V and g_A are known. At this point, we could actually apply the same procedure as being used in subsection 1.1.2 for the interaction term (2.2.13) to find the vertex factor and the result is as follows:



$$\text{Diagram} = \frac{i}{2} (g_V \gamma^\mu - g_A \gamma^\mu \gamma^5) \quad (2.2.14)$$

In fact, this result holds for all other species of fermions with the corresponding coupling constants g_V and g_A provided in table (2.2).

Fermions	g_V	g_A
$\nu_e \nu_\mu \nu_\tau$	$\frac{g}{2c_W}$	$\frac{g}{2c_W}$
$e \mu \tau$	$-\frac{g}{2c_W}(1 - 4s_W^2)$	$-\frac{g}{2c_W}$
$u c t$	$\frac{g}{c_W} \left(\frac{1}{2} - \frac{4}{3}s_W^2 \right)$	$\frac{g}{2c_W}$
$d s b$	$\frac{g}{c_W} \left(-\frac{1}{2} + \frac{2}{3}s_W^2 \right)$	$-\frac{g}{2c_W}$

 Table 2.2: Coupling constants of weak interaction mediated by Z boson

2.3 The propagator of Z -boson

The next thing to do is to find the propagator of Z -boson. Now, we have to first go back to insert (2.2.2) into the gauge field Lagrangian in equation (2.1.8) and try to pull out the kinetic term for Z_μ . Notice that since we are interested in the Lagrangian of free Z_μ only, any interaction terms that contain products of two gauge fields and their derivatives or four gauge fields should be excluded. That will leave us with:

$$\mathcal{L}_Z^{kin} = -\frac{1}{4}(\partial_\mu Z_\nu - \partial_\nu Z_\mu)(\partial^\mu Z^\nu - \partial^\nu Z^\mu). \quad (2.3.1)$$

However, this is not yet the complete Lagrangian of free Z_μ , since there is a mass term of Z_μ hidden in the kinetic part of the Higgs Lagrangian and also we have the gauge fixing term:

$$\left\{ \begin{array}{l} \mathcal{L}_Z^{mass} = \frac{1}{2}m_Z^2 Z_\mu Z^\mu \\ \mathcal{L}_Z^{gf} = \frac{1}{2\xi}(\partial^\mu Z_\mu)^2 \end{array} \right. \quad (2.3.2)$$

From (2.3.1) and (2.3.2), we have:

$$\mathcal{L}_Z = -\frac{1}{4}(\partial_\mu Z_\nu - \partial_\nu Z_\mu)(\partial^\mu Z^\nu - \partial^\nu Z^\mu) + \frac{1}{2}m_Z^2 Z_\mu Z^\mu + \frac{1}{2\xi}(\partial^\mu Z_\mu)^2. \quad (2.3.3)$$

The corresponding Euler-Lagrange equation for (2.3.3) will be:

$$\left[(\square + m_Z^2)g^{\mu\rho} - \left(1 - \frac{1}{\xi}\right) \partial^\mu \partial^\rho \right] D_{\rho\nu}(x-y) = g_\nu^\mu \delta^4(x-y). \quad (2.3.4)$$

By switching into using the propagator in phase space $D_{\rho\nu}(k)$, we will have:

$$\left[(-q^2 + m_Z^2)g^{\mu\rho} + \left(1 - \frac{1}{\xi}\right) q^\mu q^\rho \right] D_{\rho\nu}(q) = g_\nu^\mu. \quad (2.3.5)$$

At this point, we could repeat the procedure that has been introduced in subsection (1.1.1) since the form of (2.3.5) is quite similar to the form of (1.1.9), we shall have:

$$D_{\rho\nu}(q) = \frac{1}{q^2 - m_Z^2} \left[-g_{\rho\nu} + \frac{q_\rho q_\nu}{q^2 - \xi m_Z^2} (1 - \xi) \right]. \quad (2.3.6)$$

Essentially, we have to note that the gauge fixing constant of Z -boson propagator in (2.3.6) is actually the same as the one of the photon propagator in (1.1.12). Previously in QED, we proved that the amplitude is independent to the gauge we used, this feature, however, only stay true for SM in case we consider also the amplitude of diagrams with H and χ_3 . Fortunately, by setting $m_e = 0$, the diagrams involving H and χ_3 vanish, and therefore we have the cancellation of ξ as in the case of QED. Nevertheless, from now on, we shall choose to work specifically in Feynman gauge where $\xi = 1$.

Let's now discuss the Z -boson propagator a bit in details. As could be seen, there is the factor $\frac{1}{q^2 - m_Z^2}$, this pattern is actually a general feature of all the vector fields and even scalar field propagators. That is to say there is always a factor of the form $\frac{1}{s - m^2}$ for the scattering process of type $e^- + e^+ \longrightarrow f + \bar{f}$ (notice that $q^2 = s$ for the respective process) with m is the mass of the corresponding fields. It is however more important to note that this factor would guarantee a peak at the point where $\sqrt{s} = m$ in the plot of total cross-section with respect to energy in CM frame if $m > 2m_f$, since the propagator contributes directly to the squared amplitude and hence to the total cross-section itself. Unfortunately, that will lead to a divergence in the total cross-section since m is real, this feature is unexpected and could not be realistic. The reason for such divergence is because we have considered only the lowest order of approximation for the propagators (using only the Lagrangian of free Z_μ). If higher order terms are taken into account, we will then have the so-called Breit-Wigner propagator. In Feynman gauge, for Z -boson, the corresponding Breit-Wigner propagator is:

$$D_{\rho\nu}(q) = \frac{-g_{\rho\nu}}{q^2 - m_Z^2 + i\Gamma_Z m_Z} \quad (2.3.7)$$

Here, Γ_Z is the decay width of Z boson, the calculation of Γ_Z could be done theoretically, but it is not really necessary here. Thus, we will just take the experimental value of Γ_Z ($\Gamma_Z \simeq 2.4952$ GeV) for later calculation.

2.4 The Feynman amplitude

With the propagators and the vertex factors obtained we are now able to write down the Feynman amplitude for the scattering process $e^- + e^+ \longrightarrow \mu^- + \mu^+$. The Feynman rules are essentially the same as before, but for the internal lines of Z -boson, we need to replace the photon propagator by the new Z -boson propagator as in equation (2.3.7). Also, in the case of processes mediated by Z -boson, the vertex factor in the case of QED in (1.1.16) must be replaced by the one for weak interaction in (2.2.14). Now, looking at the two diagrams in figure (2.1) and applying the rules in Feynman gauge, we shall have:

$$\mathcal{M} = \mathcal{M}_\gamma + \mathcal{M}_Z. \quad (2.4.1)$$

Where \mathcal{M}_γ and \mathcal{M}_Z are:

$$\mathcal{M}_\gamma = [\bar{v}_{s'}(p')(ie\gamma^\mu)u_s(p)] \left(-\frac{g_{\mu\nu}}{q^2} \right) [\bar{u}_r(k)(ie\gamma^\nu)v_{r'}(k')], \quad (2.4.2)$$

$$\begin{aligned} \mathcal{M}_Z &= \left[\bar{v}_{s'}(p') \frac{i}{2} (g_V \gamma^\mu - g_A \gamma^\mu \gamma^5) u_s(p) \right] \left(-\frac{g_{\mu\nu}}{q^2 - m_Z^2 + i\Gamma_Z m_Z} \right) \\ &\quad \times \left[\bar{u}_r(k) \frac{i}{2} (g_V \gamma^\nu - g_A \gamma^\nu \gamma^5) v_{r'}(k') \right]. \end{aligned} \quad (2.4.3)$$

Again, we have to stress that there should be more mediators for such process. In Feynman gauge, we have also H -the Higgs particle and χ_3 -the neutral Goldstone boson. However, the vertex factor of both eeH and $ee\chi_3$ are proportional to m_e and in our calculation we normally set $m_e = 0$. Hence, diagrams involving those mediators could be omitted.

Now, with the formula (2.4.1), (2.4.2), and (2.4.3), we are able to write down the squared amplitude:

$$|\mathcal{M}_0|^2 = |\mathcal{M}_1|^2 + |\mathcal{M}_2|^2 + |\mathcal{M}_3|^2, \quad (2.4.4)$$

In which we have

$$\begin{aligned} |\mathcal{M}_1|^2 &= \frac{1}{(s - m_Z^2)^2 + \Gamma_Z^2 m_Z^2} \left[\frac{1}{2} g_V^4 (p' \cdot k)(p \cdot k') + \frac{1}{2} g_V^4 (p \cdot k)(p' \cdot k') \right. \\ &\quad \left. + 3g_A^2 g_V^2 (p' \cdot k)(p \cdot k') - g_A^2 g_V^2 (p \cdot k)(p' \cdot k') + \frac{1}{2} g_A^4 (p' \cdot k)(p \cdot k') \right. \\ &\quad \left. + \frac{1}{2} g_A^4 (p \cdot k)(p' \cdot k') + \frac{1}{2} m_\mu^2 g_V^4 (p \cdot p') - \frac{1}{2} m_\mu^2 g_A^4 (p \cdot p') \right], \end{aligned} \quad (2.4.5)$$

$$\begin{aligned} |\mathcal{M}_2|^2 &= \frac{e^2}{s(s - m_Z^2 + i\Gamma_Z m_Z)} [2g_V^2 (p' \cdot k)(p \cdot k') + 2g_V^2 (p \cdot k)(p' \cdot k') \\ &\quad + 2g_A^2 (p' \cdot k)(p \cdot k') - 2g_A^2 (p \cdot k)(p' \cdot k') + 2m_\mu^2 g_V^2 (p \cdot p')] \\ &\quad + \frac{e^2}{s(s - m_Z^2 - i\Gamma_Z m_Z)} [2g_V^2 (p' \cdot k)(p \cdot k') + 2g_V^2 (p \cdot k)(p' \cdot k') \\ &\quad + 2g_A^2 (p' \cdot k)(p \cdot k') - 2g_A^2 (p \cdot k)(p' \cdot k') + 2m_\mu^2 g_V^2 (p \cdot p')], \end{aligned} \quad (2.4.6)$$

$$|\mathcal{M}_3|^2 = \frac{e^4}{q^4} [8(p' \cdot k)(p \cdot k') + 8(p \cdot k)(p' \cdot k') + 8m_\mu^2 (p \cdot p')]. \quad (2.4.7)$$

Now, notice that we use the symbol \mathcal{M}_0 instead of \mathcal{M} , this is because to derive the formula (2.4.4) we have to take the average over the initial spin indices and sum over the final spin indices. In mathematical language, it means:

$$|\mathcal{M}_0|^2 = \frac{1}{4} \sum_{s,s',r,r'} \mathcal{M} \mathcal{M}^\dagger, \quad (2.4.8)$$

Furthermore, we have to stress that the calculation above was done with aid of FORM².

²FORM is a symbolic manipulation system that could help to perform trace calculation which is of great help for calculating the Feynman amplitude. In this thesis, most of the amplitude calculations were done using FORM version 4.1 (for further reading, see [4]).

At this point, we could simply choose to work specifically in CM frame like what we have done in chapter 1 and insert the kinematic relations in (1.2.14) into (2.4.4) to obtain the squared amplitude as a function of θ , we shall have:

$$|\mathcal{M}_1|^2 = \frac{E^2}{(s - m_Z^2)^2 + \Gamma_Z^2 m_Z^2} \left[(g_V^2 + g_A^2)^2 (E^2 + |\vec{k}|^2 \cos^2 \theta) + (g_V^4 - g_A^4) m_\mu^2 + 8g_A^2 g_V^2 E |\vec{k}| \cos \theta \right], \quad (2.4.9)$$

$$|\mathcal{M}_2|^2 = \frac{8e^2 (s - m_Z^2) E^2}{s[(s - m_Z^2)^2 + \Gamma_Z^2 m_Z^2]} [g_V^2 (E^2 + m_\mu^2 + |\vec{k}|^2 \cos^2 \theta) + 2g_A^2 E |\vec{k}| \cos \theta], \quad (2.4.10)$$

$$|\mathcal{M}_3|^2 = \frac{16e^4 E^2}{s^2} (E^2 + m_\mu^2 + |\vec{k}|^2 \cos^2 \theta). \quad (2.4.11)$$

Because the formula of $|\mathcal{M}_0|^2$ is quite lengthy to be written down repeatedly, we will transform it a bit. Let's first denote $\mu = m_\mu^2/E^2$ and then introduce the factor χ_0 :

$$\chi_0(s) = \frac{s}{4e^2(s - m_Z^2 + i\Gamma_Z m_Z)} \Rightarrow \begin{cases} \frac{1}{(s - m_Z^2)^2 + \Gamma_Z^2 m_Z^2} = \frac{16e^4}{s^2} |\chi_0(s)|^2 \\ \frac{s - m_Z^2}{(s - m_Z^2)^2 + \Gamma_Z^2 m_Z^2} = \frac{4e^2}{s} \text{Re}\chi_0(s) \end{cases} \quad (2.4.12)$$

With these factors we could actually simplify (2.4.9), (2.4.10), and (2.4.11) into:

$$|\mathcal{M}_1|^2 = \frac{16e^4 E^2}{s^2} |\chi_0|^2 \left[(g_V^2 + g_A^2)^2 (E^2 + |\vec{k}|^2 \cos^2 \theta) + (g_V^4 - g_A^4) m_\mu^2 + 8g_A^2 g_V^2 E |\vec{k}| \cos \theta \right] \quad (2.4.13)$$

$$|\mathcal{M}_2|^2 = \frac{16e^4 E^2}{s^2} \text{Re}\chi_0 [2g_V^2 (E^2 + m_\mu^2 + |\vec{k}|^2 \cos^2 \theta) + 4g_A^2 E |\vec{k}| \cos \theta] \quad (2.4.14)$$

$$|\mathcal{M}_3|^2 = \frac{16e^4 E^2}{s^2} (E^2 + m_\mu^2 + |\vec{k}|^2 \cos^2 \theta) \quad (2.4.15)$$

Now, we could write down a more compact form of $|\mathcal{M}_0|^2$:

$$|\mathcal{M}_0|^2 = \frac{16e^4 E^2}{s^2} \left[G_1(s) |\vec{k}|^2 \cos^2 \theta + G_2(s) E^2 + G_3(s) 4E |\vec{k}| \cos \theta \right] \quad (2.4.16)$$

In which we have:

$$G_1(s) = (g_V^2 + g_A^2)^2 |\chi_0(s)|^2 + 2g_V^2 \text{Re}\chi_0(s) + 1 \quad (2.4.17)$$

$$G_2(s) = [(g_V^2 + g_A^2)^2 + (g_V^4 - g_A^4)\mu] |\chi_0(s)|^2 + 2g_V^2 \text{Re}\chi_0(s)(\mu + 1) + \mu + 1 \quad (2.4.18)$$

$$G_3(s) = 2g_A^2 g_V^2 |\chi_0(s)|^2 + g_A^2 \text{Re}\chi_0(s) \quad (2.4.19)$$

The formula (2.4.16) is not only a more compressed expression mathematically but also present more clearly the symmetric and antisymmetric parts of $|\mathcal{M}_0|^2$ with respect to $\cos \theta$. In the following subsections where some quantities of interest are studied, we shall see that the asymmetry of $|\mathcal{M}_0|^2$ emerging from the approach of SM which adopt also Z -boson as a mediator will lead to some very profoundly different features between QED and SM.

2.4.1 The forward-backward asymmetry

The very first quantity we would like to analyse is the total cross-section. For muon pair creation in electron positron scattering process, we have:

$$\begin{aligned} \frac{d\sigma}{d\Omega} &= \frac{1}{64\pi^2} \frac{|\mathcal{M}_0|^2}{(E_{e^-} + E_{e^+})^2} \frac{|\vec{k}|}{|\vec{p}|} \\ \Rightarrow \frac{d\sigma}{d(\cos\theta)} &= -\frac{e^4 |\vec{k}|}{8\pi E s^2} \left[G_1(s) |\vec{k}|^2 \cos^2\theta + G_2(s) E^2 + G_3(s) 4E |\vec{k}| \cos\theta \right]. \end{aligned} \quad (2.4.20)$$

Thus, the total cross-section will be:

$$\sigma_T = \int_1^{-1} \frac{d\sigma}{d(\cos\theta)} d(\cos\theta) = \frac{|\vec{k}| e^4}{4\pi E s^2} \left[G_1(s) \frac{|\vec{k}|^2}{3} + G_2(s) E^2 \right]. \quad (2.4.21)$$

In figure (2.2), we could see that in low energy range the total cross-section in case of SM seems to be not much different from that of QED. However, at higher energy range, we could see a very sharp peak at roughly about 90 GeV. This is definitely the sign of Z -boson since there are terms with factors of the form $\frac{1}{(s-m_Z)^2 + \Gamma_{Zm_Z}}$ within $|\mathcal{M}_0|^2$.

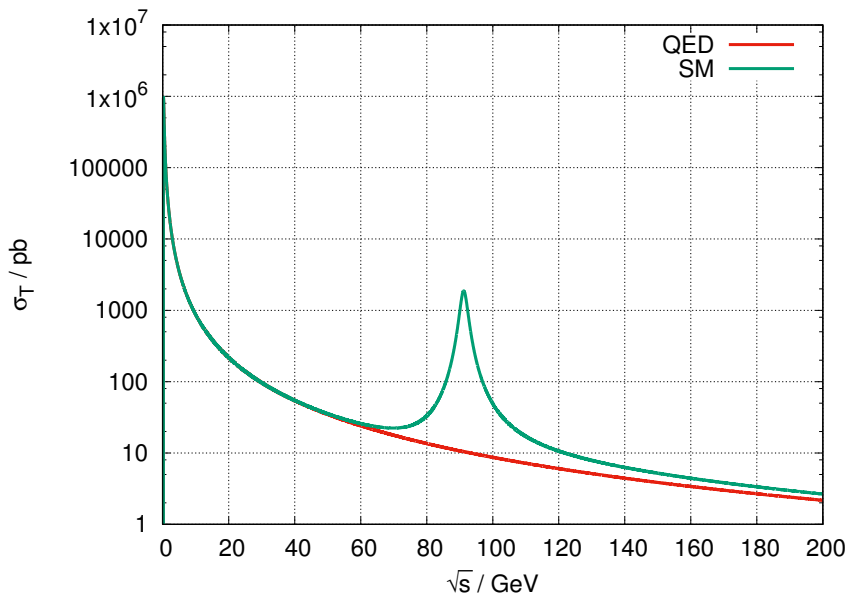


Figure 2.2: Total cross-section

Now, let's continue with the angular distribution with the formula presented in equation (2.4.20). The difference we will see here is even more profound. The plots for the angular distribution in both cases QED and SM with total energy in CM frame as about 200 GeV are shown in figure (2.3a). The red line is the original result of QED and as we have discussed before it is perfectly symmetric. As for the green line which is the angular distribution in the case of SM, the pattern of asymmetry has been depicted very clearly. From this we can say that when we consider also Z -boson as a mediator at high CM energy, muons are more likely to come out forward.

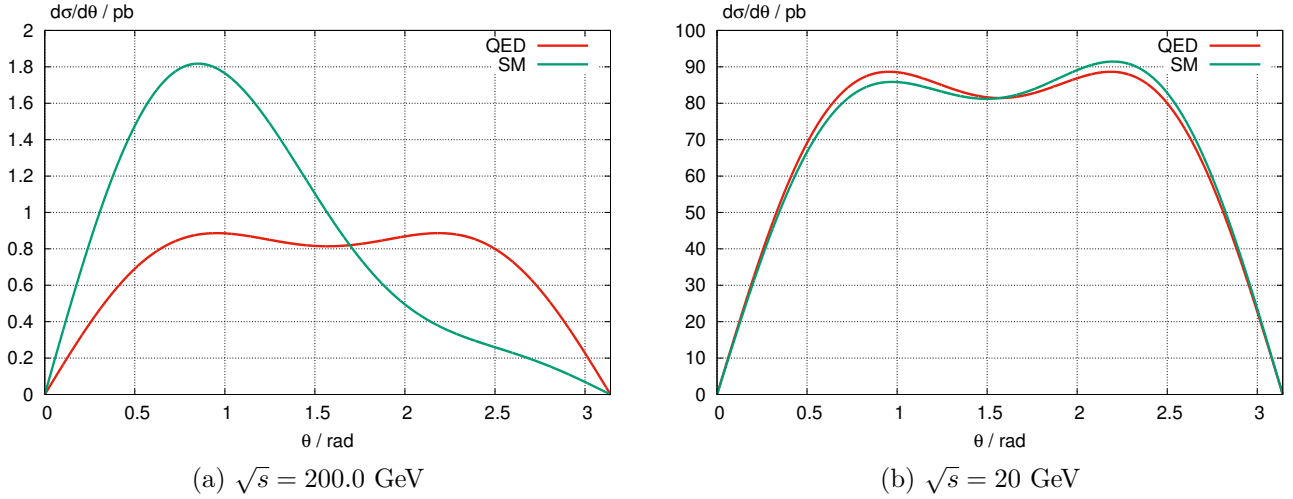


Figure 2.3: The angular distribution

To evaluate how asymmetric it is, physicists introduced a quantity called the forward-backward asymmetry denoted as A_{FB} and defined as:

$$A_{FB} = \frac{\sigma_F - \sigma_B}{\sigma_F + \sigma_B} = \frac{\sigma_{FB}}{\sigma_T}. \quad (2.4.22)$$

Here we have:

$$\begin{cases} \sigma_F = \int_0^{\frac{\pi}{2}} \frac{d\sigma}{d\theta} d\theta \\ \sigma_B = \int_{\frac{\pi}{2}}^{\pi} \frac{d\sigma}{d\theta} d\theta \end{cases} \quad (2.4.23)$$

Let's now deduce the explicit form of σ_F , σ_B , and A_{FB} , we have:

$$\begin{aligned} \sigma_F &= \int_0^{\frac{\pi}{2}} \frac{d\sigma}{d\theta} d\theta = \frac{|\vec{k}|e^4}{8\pi E s^2} \left[G_1(s) \frac{|\vec{k}|^2}{3} + G_2(s) E^2 + G_3(s) 2E |\vec{k}| \right] \\ \sigma_B &= \int_{\frac{\pi}{2}}^{\pi} \frac{d\sigma}{d\theta} d\theta = \frac{|\vec{k}|e^4}{8\pi E s^2} \left[G_1(s) \frac{|\vec{k}|^2}{3} + G_2(s) E^2 - G_3(s) 2E |\vec{k}| \right] \\ \Rightarrow \sigma_{FB} &= \sigma_F - \sigma_B = \frac{|\vec{k}|e^4}{8\pi E s^2} G_3(s) 4E |\vec{k}| = \frac{|\vec{k}|^2 e^4}{2\pi s^2} G_3(s) \end{aligned} \quad (2.4.24)$$

From (2.4.24) and (2.4.21), we have:

$$A_{FB} = \frac{\sigma_{FB}}{\sigma_T} = \frac{6G_3(s)\sqrt{1-\mu}}{G_1(s)(1-\mu) + 3G_2(s)} \quad (2.4.25)$$

From the formula above, we could actually plot A_{FB} with respect to \sqrt{s} (see figure (2.4)). Generally speaking, it seems that the results in (2.4) matched with the physical interpretation seen from figure (2.3). At high energy range, with $\sqrt{s} = 200 \text{ GeV}$ (figure (2.3a)), for example, we could clearly see that $A_{FB} > 0$.

However, when we set it back to low energy scale where QED phenomena dominate. As we put $\sqrt{s} = 20.0$ GeV, we will have the plots in figure (2.3b), the angular distribution of SM seems to present quite the same pattern as that of QED since we also have two peaks at around $\theta = 0.95$ rad and $\theta = 2.19$ rad. This again confirms our understanding that QED is actually just a special case of SM at low energy scale. Nevertheless, the forward-backward asymmetry is still there in the distribution in figure (2.3b) and we could see that in this case $A_{FB} < 0$.

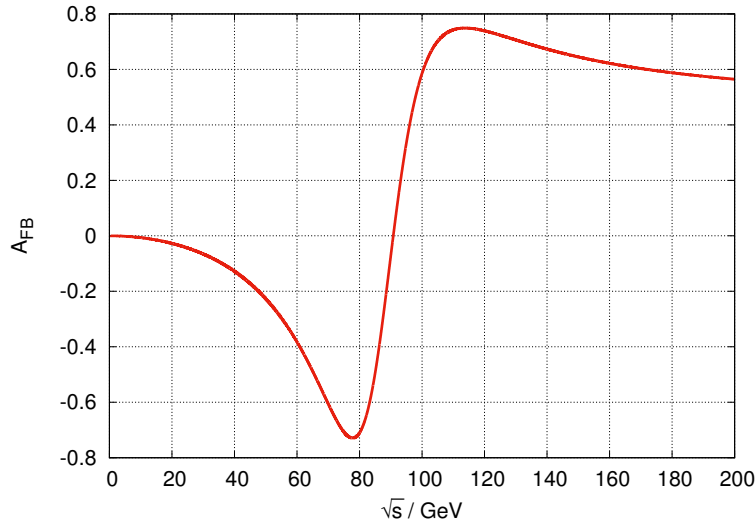


Figure 2.4: A_{FB} with respect to \sqrt{s}

2.4.2 Transverse momentum and longitudinal momentum distributions and rapidity distribution of muon

The transverse momentum distribution could be derived by following the same procedure used in subsection 1.3.3, we shall have:

$$\frac{d\sigma}{dk_t} = \frac{d\sigma}{d\theta} = \sum_i \frac{d\sigma}{d\theta} \Big|_{\theta=\theta_i} \left| \frac{d\theta}{dk_t} \Big|_{\theta=\theta_i} \right| \quad (2.4.26)$$

With θ_i ($i = \overline{1,2}$) provided in (1.3.5). For the transverse momentum distribution in the case of SM, the main features are essentially the same as in the case of QED as could be seen in figure (2.5a).

Another quantity of interest is the longitudinal momentum distribution. The longitudinal momentum distribution will take the form:

$$\frac{d\sigma}{dk_l} = \frac{d\sigma}{d\theta} \Big|_{\theta=\arccos \frac{k_l}{|\vec{k}|}} \left| \frac{d\theta}{dk_l} \Big|_{\theta=\arccos \frac{k_l}{|\vec{k}|}} \right| \quad (2.4.27)$$

Again, the forward-backward asymmetry—a profound difference between SM and QED has been depicted in the plots of longitudinal momentum distributions in figure (2.5b). The distribution at $\sqrt{s} = 200$ GeV is higher in the range of positive values of longitudinal

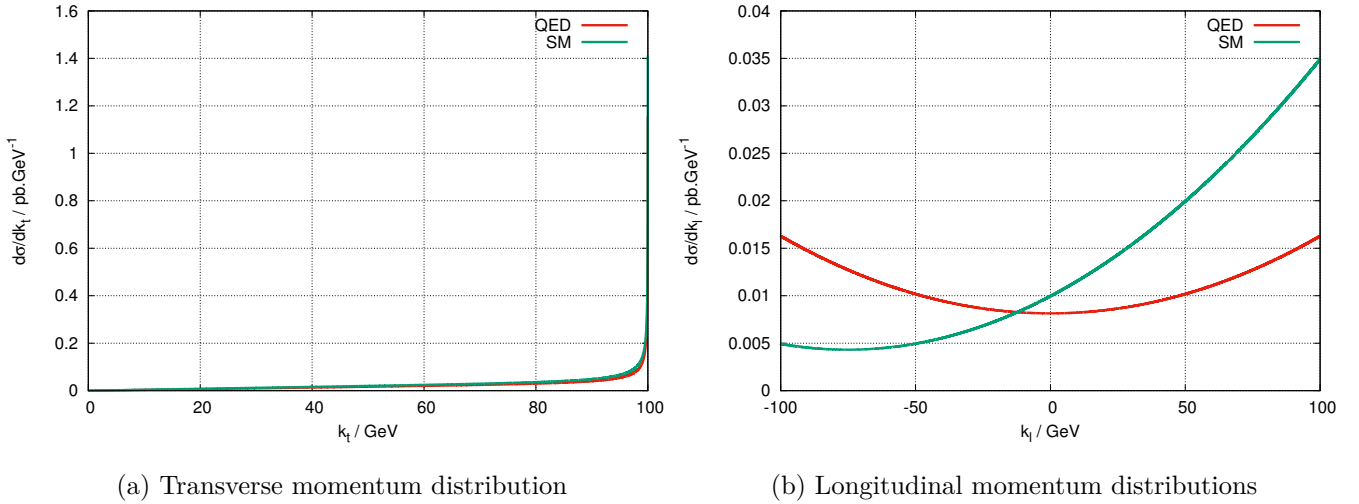


Figure 2.5: Transverse and longitudinal momentum distributions with $\sqrt{s} = 200.0$ GeV

momentum. This feature is exactly in accordance to what we have seen in the angular distribution.

Last but not least, we shall have a look at rapidity distribution as being discussed in subsection 1.3.4, rapidity is preferable by experimentalists due to its law of transformation under boosts. We have:

$$\frac{d\sigma}{dy} = \frac{d\sigma}{dk_l} \bigg|_{k_l = E \tanh y} \left| \frac{dk_l}{dy} \right|_{k_l = E \tanh y}. \quad (2.4.28)$$

With the formula (2.4.28) we have the resulting plot of the rapidity distribution illustrated in figure (2.6). Here, we could see that the forward-backward asymmetry causes a shift toward positive values of rapidity and again this means we have greater probability to see muon coming out forwards.

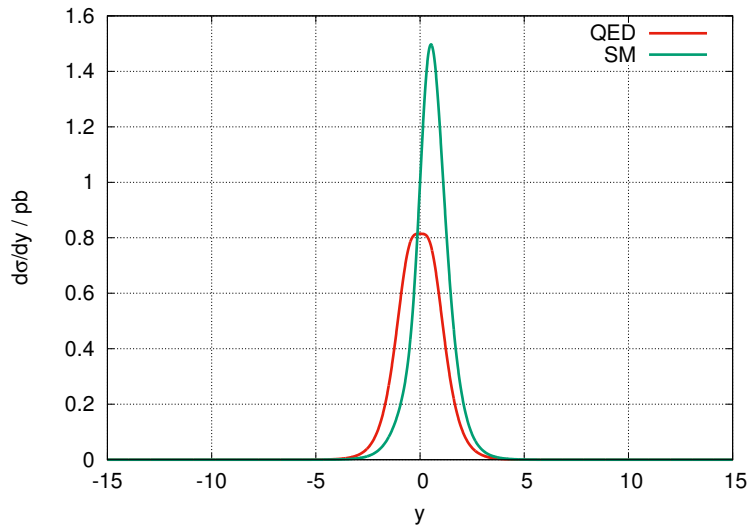


Figure 2.6: The rapidity distribution with $\sqrt{s} = 200.0$ GeV

Chapter 3

Initial state QED correction

So far, we have been studying the scattering process $e^- + e^+ \rightarrow \mu^- + \mu^+$ quite intensively. However, what we have done is just simply the lowest order of approximation. To be more precise we need to consider also some higher-order diagrams for example second order vertex modification at initial state or electron and positron self-energy loop. More importantly, we do have to consider also the phenomena of soft photon emission from both electron and positron in order to compare the theoretical results obtained with the experimental ones.

In SM, those corrections at next-to-leading-order correspond to 10 diagrams presented in figure (3.1). Considered together, they are called initial state QED correction and in this final chapter we shall take into account this correction¹.

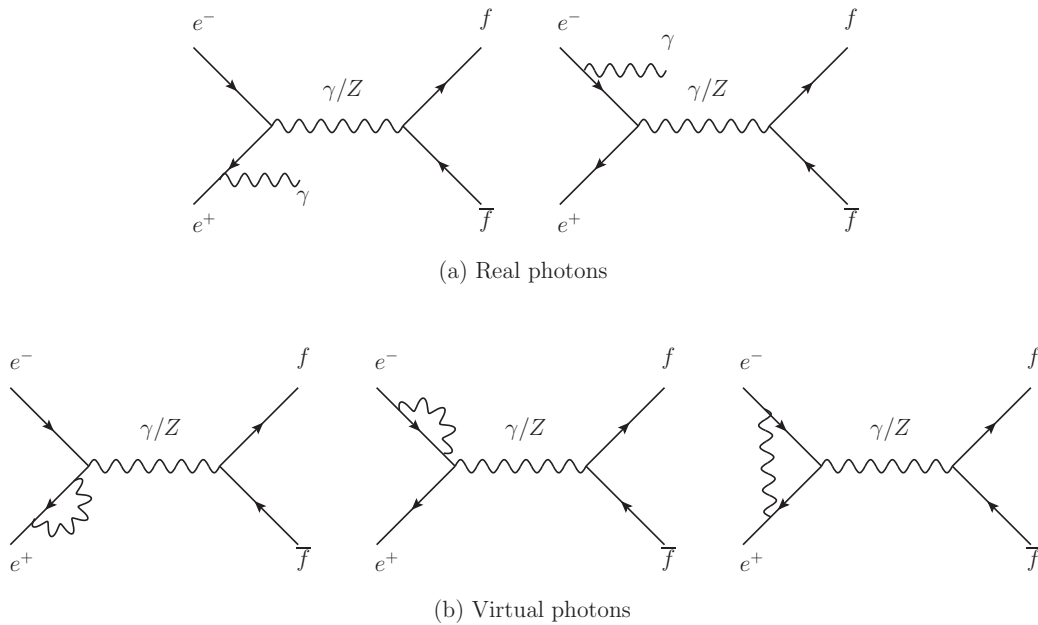


Figure 3.1: Feynman diagrams of initial state QED correction in SM

¹In fact, there are also final state and initial-final interference QED corrections (see [5] for further discussion). It is, however, more preferable to first concentrate on initial state correction as its contribution to the reduction of the height of the Z -boson peak is more prominent (roughly 40%).

Nevertheless, at the beginning of this chapter, let's first generalise the analytical formulas of several quantities of interest obtained in the previous chapter by considering a more general scattering process $e^- + e^+ \rightarrow f + \bar{f}$ ($f \neq e$). Those formulas will indeed allow us to provide a more general results with QED correction for later analysis of some interesting cases like $f = c$ or $f = b$.

3.1 The scattering process $e^- + e^+ \rightarrow f + \bar{f}$

As being discussed in chapter 2, we will particularly concentrate on the two diagrams with photon and Z -boson as mediators only.

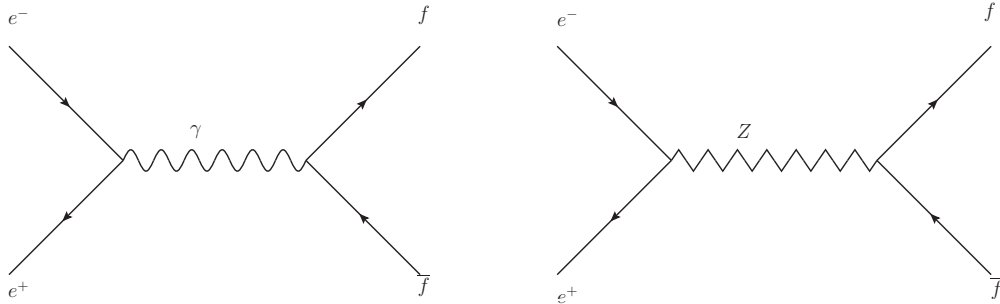


Figure 3.2: The Feynman diagrams of $e^- + e^+ \rightarrow f + \bar{f}$ in SM

Again, let's denote the momenta and the spin indices of e^- , e^+ , f , and \bar{f} to be (p,s) , (p',s') , (k,r) and (k',r') correspondingly and then write down the Feynman amplitude for this process with the choice of gauge is again the Feynman gauge:

$$\mathcal{M} = \mathcal{M}_\gamma + \mathcal{M}_Z. \quad (3.1.1)$$

Here, we have:

$$\mathcal{M}_\gamma = v_{s'}(p') (iQ_e e \gamma^\alpha) u_s(p) \left(-\frac{g_{\mu\nu}}{q^2} \right) u_r(k) (iQ_f e \gamma^\beta) v_{r'}(k'), \quad (3.1.2)$$

$$\begin{aligned} \mathcal{M}_Z &= \left[v_{s'}(p') \frac{i}{2} (g_{eV} \gamma^\nu - g_{eA} \gamma^\nu \gamma^5) u_s(p) \right] \left(-\frac{g_{\mu\nu}}{s - m_Z^2 + i\Gamma_Z m_Z} \right) \\ &\quad \times \left[u_r(k) \frac{i}{2} (g_{fV} \gamma^\nu - g_{fA} \gamma^\nu \gamma^5) v_{r'}(k') \right]. \end{aligned} \quad (3.1.3)$$

Here, we have Q_f , g_{fV} , and g_{fA} are respectively the charge and the coupling constants of the particle f . Now, we shall take the square of \mathcal{M} , average over the initial states, sum over the final states, and finally insert the kinematic relations for this process in CM frame (presented in (1.2.14)). The procedure is quite similar to the one presented in the previous chapter. Thus, we shall write down the result directly:

$$|\mathcal{M}_0|^2 = \frac{16e^4 E^2}{s^2} \left[G_1(s) |\vec{k}|^2 \cos^2 \theta + G_2(s) E^2 + G_3(s) 4E |\vec{k}| \cos \theta \right], \quad (3.1.4)$$

In which we have:

$$G_1(s) = N_c \left[(g_{eV}^2 + g_{eA}^2)(g_{fV}^2 + g_{fA}^2) |\chi_0(s)|^2 + 2Q_e Q_f g_{eV} g_{fV} \text{Re} \chi_0(s) + Q_e^2 Q_f^2 \right], \quad (3.1.5)$$

$$G_2(s) = N_c \left\{ [(g_{eV}^2 + g_{eA}^2)(g_{fV}^2 + g_{fA}^2) + (g_{eV}^2 + g_{eA}^2)(g_{fV}^2 - g_{fA}^2)\mu] |\chi_0(s)|^2 + 2Q_e Q_f g_{eV} g_{fV} \text{Re} \chi_0(s)(\mu + 1) + Q_e^2 Q_f^2 (\mu + 1) \right\}, \quad (3.1.6)$$

$$G_3(s) = N_c \left[2g_{eV} g_{eA} g_{fV} g_{fA} |\chi_0(s)|^2 + Q_e Q_f g_{eA} g_{fA} \text{Re} \chi_0(s) \right]. \quad (3.1.7)$$

Notice that we have introduced a new factor N_c ($N_c = 1$ for leptons and $N_c = 3$ for quarks since they have three possible color states). Also, we have used the conventions $\mu = m_f^2/E^2$ and the factor $\chi_0(s)$ set in (2.4.12). At this point, we could see that the squared amplitude $|\mathcal{M}_0|^2$ in the formula (3.1.4) is different from the one (2.4.16) since the three functions $G_1(s)$, $G_2(s)$, and $G_3(s)$ are now generalised. However, they both have the same form, we could, therefore, reuse the results of σ_T , σ_{FB} , and A_{FB} at lowest order² derived in section 2.4 (formula (2.4.21), (2.4.24), and (2.4.25) correspondingly):

$$\sigma_T^{(0)} = \frac{|\vec{k}|e^4}{4\pi E s^2} \left[G_1(s) \frac{|\vec{k}|^2}{3} + G_2(s) E^2 \right], \quad (3.1.8)$$

$$\sigma_{FB}^{(0)} = \frac{|\vec{k}|^2 e^4}{2\pi s^2} G_3(s), \quad (3.1.9)$$

$$A_{FB}^{(0)} = \frac{\sigma_{FB}}{\sigma_T} = \frac{6G_3(s)\sqrt{1-\mu}}{G_1(s)(1-\mu) + 3G_2(s)}. \quad (3.1.10)$$

The results of $\sigma_T^{(0)}(s)$ and $A_{FB}^{(0)}(s)$ have been checked and perfectly matched the ones presented in [5]. Besides, we should notice that from now on the results at lowest order and the ones with initial state QED correction will be respectively labelled with the upper indices (0) and (1).

3.2 Initial state QED correction

Normally, we have to deduce the Feynman amplitude for 10 diagrams in figure (3.1) before calculating all the quantities of interest. However, that would require an extensive amount of calculation with advanced mathematical techniques. Thus, in this section, what we would like to do is to exploit the analytical formulas of the total cross-section and the forward-backward asymmetry derived in [5] for our calculation. This means that we only have to understand those results and then keep on with numerical evaluation using tools like Mathematica or C++. Now, as we know, charged particles could radiate photons at various frequencies while accelerating, that will cause energy loss and hence:

$$s \longrightarrow s' = zs, \quad (3.2.1)$$

With z must be in the range $[4m_f^2/s, 1]$. We could see that $z = 1$ corresponds to the case with no emission at all since $\sqrt{s'} = \sqrt{s}$. As for $z = 4m_\mu^2/s$, it is actually the situation

²In this case, the term "lowest order" used to refer to results with the contribution of only two diagrams in figure (3.2)

when muons have no kinetic energy after pair creation ($\sqrt{s'} = 2m_\mu$). With the above definition of z , we have the so-called radiator function $H_e^{(1)}(z)$ in the case of initial state QED correction as follows:

$$\begin{aligned}\tilde{H}_e^{(1)} &= \delta(1-z) + \frac{\alpha}{\pi} \left\{ \delta(1-z) \left[\left(2 \ln \varepsilon + \frac{3}{2} \right) (L_e - 1) + \frac{\pi^2}{3} - \frac{1}{2} \right] \right. \\ &\quad \left. + \theta(1-\varepsilon-z) \frac{1+z^2}{1-z} \left[L_e - 1 - \ln \frac{4z}{(1+z^2)} \right] \right\} \\ &= H_e^{(1)}(z) - \theta(1-\varepsilon-z) \frac{1+z^2}{1-z} \ln \frac{4z}{(1+z^2)}.\end{aligned}\quad (3.2.2)$$

With formula (3.2.2), we have the total cross-section and the forward-backward asymmetry with QED correction are:

$$\begin{aligned}\sigma_T^{(1)}(s) &= \int_{z_0}^1 dz H_e^{(1)}(z) \sigma_T^{(0)}(zs) \\ &= \sigma_T^{(0)}(s) + \frac{\alpha}{\pi} \left[\left(2 \ln \varepsilon + \frac{3}{2} \right) (L_e - 1) + \frac{\pi^2}{3} - \frac{1}{2} \right] \sigma_T^{(0)}(s) \\ &\quad + \frac{\alpha}{\pi} (L_e - 1) \int_{z_0}^{1-\varepsilon} dz \frac{1+z^2}{1-z} \sigma_T^{(0)}(zs),\end{aligned}\quad (3.2.3)$$

$$\begin{aligned}A_{FB}^{(1)}(s) &= \frac{1}{\sigma_T(s)} \int_{z_0}^1 dz \frac{4z}{(1+z)^2} \tilde{H}_e(z) \sigma_{FB}^{(0)}(zs) \\ &= \frac{1}{\sigma_T(s)} \left\{ \sigma_{FB}^{(0)}(s) + \frac{\alpha}{\pi} \left[\left(2 \ln \varepsilon + \frac{3}{2} \right) (L_e - 1) + \frac{\pi^2}{3} - \frac{1}{2} \right] \sigma_{FB}^{(0)}(s) \right. \\ &\quad \left. + \frac{\alpha}{\pi} \int_{z_0}^{1-\varepsilon} dz \frac{4z(1+z^2)}{(1+z)^2(1-z)} \left[L_e - 1 - \ln \frac{4z}{(1+z)^2} \right] \sigma_{FB}^{(0)}(zs) \right\}.\end{aligned}\quad (3.2.4)$$

Here, we have introduced $L_e = \ln(s/m_e^2)$ and a dimensionless parameter ε (let's call it the cut-off parameter). Notice that in the final terms of the formulas above z must satisfy $1 - \varepsilon \geq z \geq 4m_\mu^2/s$. Also, as could be seen in (3.2.3) and (3.2.4), the initial integrals are finite and independent of the cut-off parameter. Therefore, ε could be understood as a technical parameter and the limit $\varepsilon \rightarrow 0$ should be taken in the end (this is also known as the no-cut case). Unfortunately, in the limit $\varepsilon \rightarrow 0$, the terms with $\ln \varepsilon$ in (3.2.3) and (3.2.4) diverge, a closer look at those formulas will, however, reveal that such divergence would eventually cancel out with another one hidden in the integration term. For instance, let's consider the integration term of $\sigma_T^{(1)}(s)$, we have:

$$\begin{aligned}\mathcal{I} &= \int_{z_0}^{1-\varepsilon} dz \frac{1+z^2}{1-z} \sigma_T^0(zs) = \int_{z_0}^{1-\varepsilon} dz \frac{f(z)}{1-z} \\ \Rightarrow \mathcal{I} &= \int_{z_0}^{1-\varepsilon} dz \frac{f(z) - f(1)}{1-z} + f(1) [\ln(1-z_0) - \ln \varepsilon].\end{aligned}\quad (3.2.5)$$

Notice that the new integrand in (3.2.5) converge as $z \rightarrow 1$ or equivalently $\varepsilon \rightarrow 0$. More importantly, by inserting (3.2.5) into (3.2.3), we will see that the divergent factor $\ln \varepsilon$ disappears. That is to say $\sigma_T^{(1)}$ remains finite even in the limit ε goes to zero. In fact, the same technique could be applied for $A_{FB}^{(1)}(s)$ to prove that it also converges in

the case of soft photon inclusion. Besides, it is not really necessary to find the complete analytical form of both $\sigma_T^{(1)}(s)$ and $A_{FB}^{(1)}(s)$ in such limit, later for ease of calculation, we shall simply choose ε to be small enough ($\varepsilon \ll 1$).

Another point to note is that in some cases for simplicity the formula (3.2.4) could be replaced by an approximated one (for further discussion, see [5]):

$$A_{FB}^{approx}(s) \simeq \frac{1}{\sigma_T(s)} \int dz H_e^{(1)}(z) \sigma_{FB}^0(zs). \quad (3.2.6)$$

Up to this point, the formulas for the total cross-section and the forward-backward asymmetry with initial state QED correction have been properly introduced. Let's now proceed with numerical evaluation³.

3.2.1 Result comparison for the case of muon

First, we would like to make a comparison between the numerical results for the no-cut case of $f = \mu$ obtained here with the one presented in [5] (notice that from now on our results will be referred to as [0]). Moreover, because the input parameters set in [5] were not quite complete, we took also some constants needed for numerical evaluation like the Fermi constant G_μ or the fine structure constant α from [6]. For the input parameters:

$$\begin{aligned} m_\mu &\simeq 0.0 \text{ GeV}, & m_Z &= 93.0 \text{ GeV}, & \Gamma_Z &= 2.5 \text{ GeV}, \\ G_\mu &= 1.166344 \cdot 10^{-5} \text{ GeV}^{-2}, & \alpha &= \frac{1}{137.03604}, & \sin^2 \theta_W &= 0.23. \end{aligned}$$

The corresponding results are provided in table (3.1) with $A_{FB}^{(0)}(s)$ and $A_{FB}^{(1)}$ obtained using (3.1.8) and (3.2.4) respectively. Essentially, even though we chose $m_\mu = 0$ for ease of calculation, z_0 was still set to be non-zero as $z_0 = 4m_\mu^2/s$ with the value of m_μ taken from experiment (this is called massless fermion approximation). Besides, we should note that the coupling constants here are calculated in a slightly different way:

$$g_V = \sqrt{4\sqrt{2}G_\mu m_Z^2 (I_\mu^3 - 2Q_\mu s_W^2)} \quad (3.2.7)$$

$$g_A = \sqrt{4\sqrt{2}G_\mu m_Z^2 I_\mu^3} \quad (3.2.8)$$

With I_μ^3 is the isospin of left-handed muons. Basically, what we did for $A_{FB}^{(1)}$ is to perform calculation using different input values of ε so as to see the numerical limits of the results. It seems that it is adequate to take $\varepsilon = 10^{-8}$ since the numerical values of $A_{FB}^{(1)}(s)$ started to converge with that choice of ε . Thus, in later calculation, we shall stick with this choice. Also, we could see that the values of $A_{FB}^{(1)}(s)$ presented here are slightly different from those in the reference material [5]. The results are however acceptable to some extent, but it is worth making another comparison to see that our calculation is actually reliable. For the input parameters:

$$m_\mu \simeq 0.0 \text{ GeV}, \quad m_Z = 92.6 \text{ GeV}, \quad \Gamma_Z = 2.6 \text{ GeV}, \quad \alpha = \frac{1}{137.03604}, \quad \sin^2 \theta_W = 0.229.$$

³All the final integration terms in the formulas (3.2.3), (3.2.4), and (3.2.6) were numerically calculated utilizing function "NIntegrate" of Mathematica 10.

The numerical values of $A_{FB}(s)$ could be found in table (3.2). Here, the results $A_{FB}^{(0)}$, A_{FB}^{approx} , and $A_{FB}^{(1)}$ are evaluated using formulas (3.1.9), (3.2.6), and (3.2.4) respectively. Again, massless fermion approximation was applied, but the coupling constants g_V and g_A here were calculated as usual⁴. Once more, we could see that the agreement between the two results was not perfect. This might suggest that due to not-the-same input parameters or some other unknown reasons. Nevertheless, the two results are close enough for us to actually proceed further.

Energy\Cases	$A_{FB}^{(0)}(s)$		$A_{FB}^{(1)}$				
	[0]	[5]	[0] ($\varepsilon = 10^{-2}$)	[0] ($\varepsilon = 10^{-4}$)	[0] ($\varepsilon = 10^{-6}$)	[0] ($\varepsilon = 10^{-8}$)	[5]
\sqrt{s}							
82.0	-69.854	-69.99	-55.767	-55.782	-55.783	-55.783	-53.08
92.5	-2.220	-2.221	-3.747	-4.355	-4.362	-4.362	-4.009
93.0	1.887	1.887	0.157	-0.422	-0.428	-0.428	-0.403
93.5	5.924	5.923	3.484	2.988	2.984	2.984	2.920
100.0	47.326	47.28	19.360	19.399	19.399	19.399	19.36

Table 3.1: Comparison with table 9 of to [5]
for $e^- + e^+ \rightarrow \mu^- + \mu^+$ with QED correction in percent

Energy\Cases	$A_{FB}^{(0)}$		A_{FB}^{approx}		$A_{FB}^{(1)}$	
	[0]	[5]	[0]($\varepsilon = 10^{-8}$)	[5]	[0] ($\varepsilon = 10^{-8}$)	[5]
\sqrt{s}						
$m_Z - 5$ GeV	-0.4225	-0.4225	-0.4235	-0.4242	-0.4218	-0.4226
m_Z GeV	0.0207	0.0207	-0.0056	-0.0056	-0.0055	-0.0055
$m_Z + 5$ GeV	-0.4028	-0.4028	0.1859	0.1860	0.1867	0.1868

Table 3.2: Comparison with table 8 of to [5]
for $e^- + e^+ \rightarrow \mu^- + \mu^+$ with QED correction

Let's keep on with a more complete picture of the case $e^- + e^+ \rightarrow \mu^- + \mu^+$ with QED correction for $\varepsilon = 10^{-8}$. In this case, we have $Q_f = Q_\mu = -1$ and the values of

⁴With the input parameter s_W^2 and α , the numerical values for g and c_W could be deduced. Then, we shall apply the formulas in table (2.2) to get the corresponding values of g_V and g_A in this case.

$g_{fV} = g_{\mu V}$ and $g_{fA} = g_{\mu A}$ are provided in table (2.2) in section 2.2.4. After taking into account the effect of radiation, the plot of total cross-section with respect to \sqrt{s} has changed significantly as could be seen in figure (3.3). In fact, the peak for Z -boson is now lower as being stressed before in the footnote (1) on page 30.

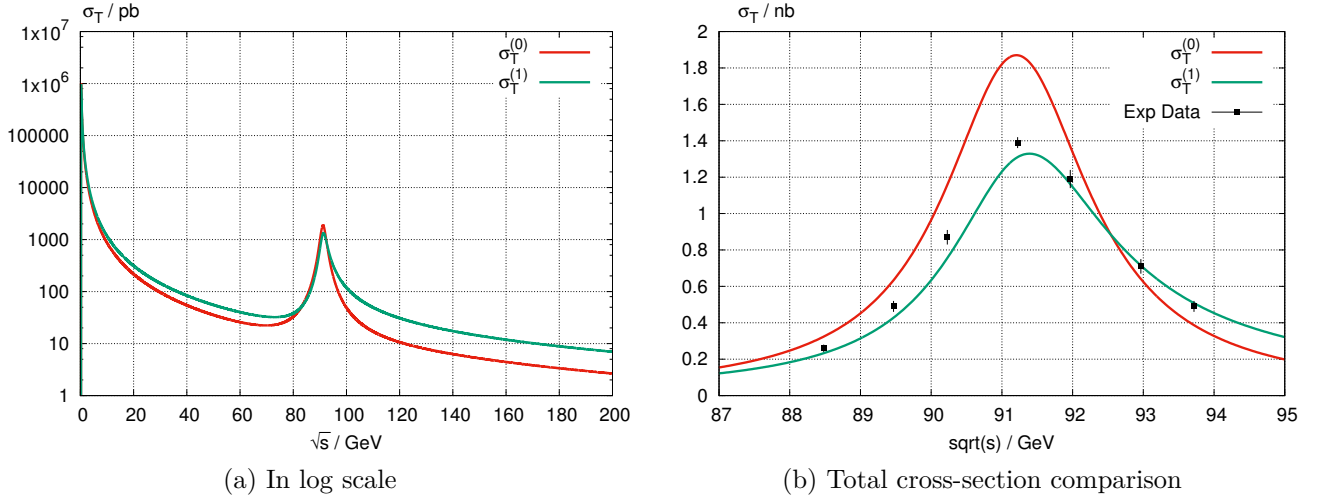


Figure 3.3: Total cross-section of $e^- + e^+ \longrightarrow \mu^- + \mu^+$ with QED correction

At this point, we would like to actually include the experimental results for comparison. In fact, the scattering process of e^- and e^+ has been experimentally analysed at the Large Electron Positron Collider (LEP). The LEP was one of the most powerful accelerators at the end of the 20th century. The data introduced here are the total cross-section and the forward-backward asymmetry from the process $e^- + e^+ \longrightarrow \mu^- + \mu^+$ taken from [7] and [8] respectively. They are, in fact, the combined results from several detectors of the LEP.

Let's first concentrate on figure (3.3b) which illustrate $\sigma_T^{(0)}$ and $\sigma_T^{(1)}$ in comparison with the experimental data (Exp Data) from [7]. As expected, the theoretical predictions of the total cross-section with initial state QED correction seems to perfectly match the experimental results.

Regarding the forward-backward asymmetry, we could see in the plot in figure (3.4a) that the differences between $A_{FB}^{(1)}$ and $A_{FB}^{(0)}$ results are quite profound, but the patterns are essentially the the same. More importantly, we could notice that again the results with QED correction are closer to the experimental results from [8]. Besides, there is one thing that we have to stress at this point is that to get the experimental results of A_{FB} from [8] we used a program called EasyNData⁵.

3.2.2 Application for the cases of b-quark and c-quark

Let's now keep on to apply the results we have obtained for the general process $e^- + e^+ \longrightarrow f + \bar{f}$ to the two cases of b-quark and c-quark. Here, the experimental results of the

⁵EasyNData is particularly designed to help extract numerical values from published plots. In fact, many sets of experimental data in this thesis were collected this way (for discussion regarding the precision of such program see [9])

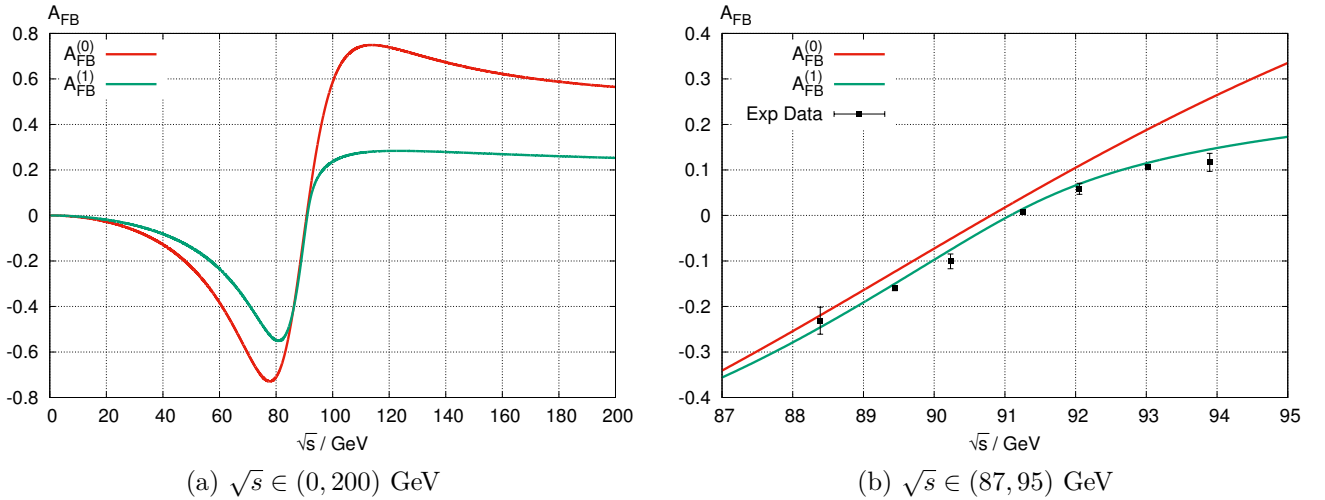


Figure 3.4: Forward-backward asymmetry

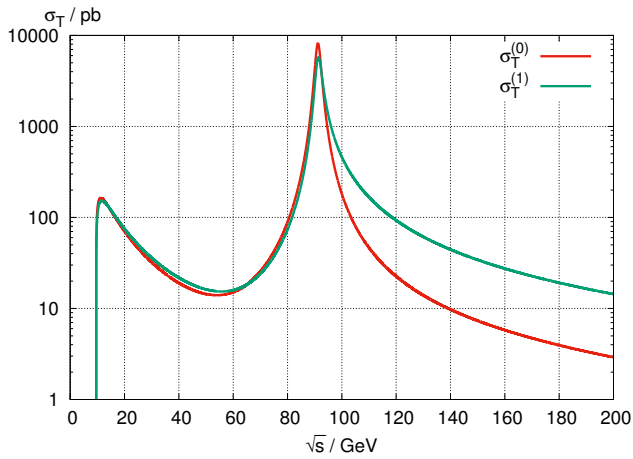
forward-backward asymmetry from LEP are also included in figure (3.5b) and (3.5d). Essentially, the pole masses of b-quark and c-quark were chosen to be $m_b = 4.78$ GeV and $m_c = 1.78$ GeV for numerical calculation. Nevertheless, it seems that for these two cases the theoretical predictions and the experimental results do not well match. Since for quark particles, the situation is more complicated. For more precise results, strong interaction effects may be important, it is, however, beyond the scope of this thesis.

Another interesting quantity we would like to discuss is the total cross-section of processes of type $e^- + e^+ \rightarrow hadrons$ around Z -peak since we also have experimental data from LEP for comparison. Those processes are mostly contributed by $e^- + e^+ \rightarrow q + \bar{q}$ (where $q = u, d, s, c, b$ since we consider only the region where $\sqrt{s} \in [87; 95]$ -around Z -peak). Hence, the total cross-section might be calculated as the following:

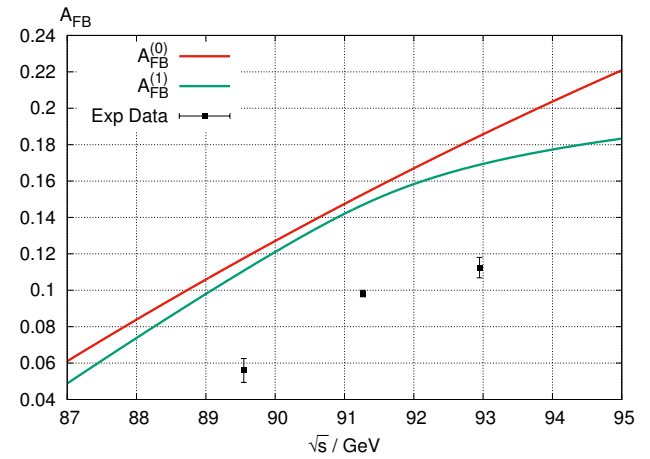
$$\sigma_{had}(s) \simeq \sum_{q=u,d,s,c,b} \sigma_q(s) \quad (3.2.9)$$

In fact, formula (3.2.9) could be applied for both cases of the result at lowest order $\sigma_q^{(0)}(s)$ and the one with QED correction $\sigma_q^{(1)}(s)$ ⁶. With the formula above, we have the plot for both $\sigma_{had}^{(0)}$ and $\sigma_{had}^{(1)}$ in comparison with experimental data in figure (3.6). It seems that the experimental results are in good agreement with the theoretical predictions of $\sigma_{had}^{(1)}(s)$ at most energy points except for the point of Z -resonance. Once again, for better agreement, QCD correction should be included.

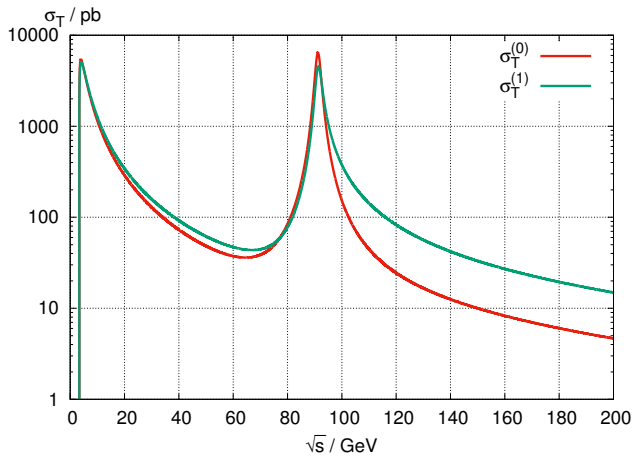
⁶Notice that in the calculation for $e^- + e^+ \rightarrow q + \bar{q}$, we used $m_u = 2.3$ MeV, $m_d = 4.8$ MeV, $m_s = 95.0$ MeV, $m_c = 1.67$ GeV, and $m_b = 4.78$ GeV.



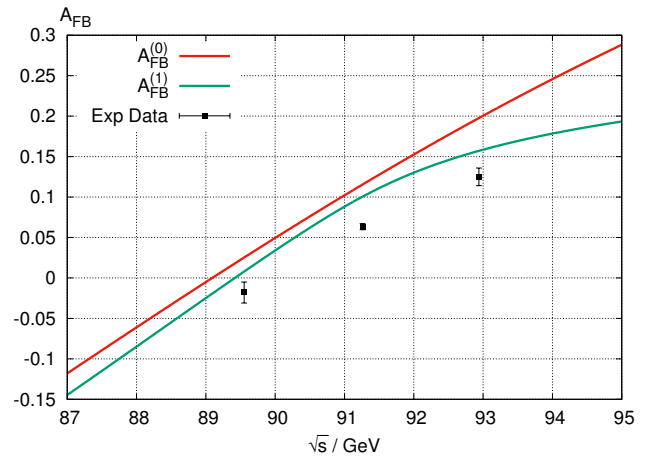
(a) Total cross section of $e^- + e^+ \rightarrow b + \bar{b}$



(b) Forward-backward asymmetry of $e^- + e^+ \rightarrow b + \bar{b}$



(c) Total cross section of $e^- + e^+ \rightarrow c + \bar{c}$



(d) Forward-backward asymmetry of $e^- + e^+ \rightarrow c + \bar{c}$

Figure 3.5: Results for the case of b-quark and c-quark

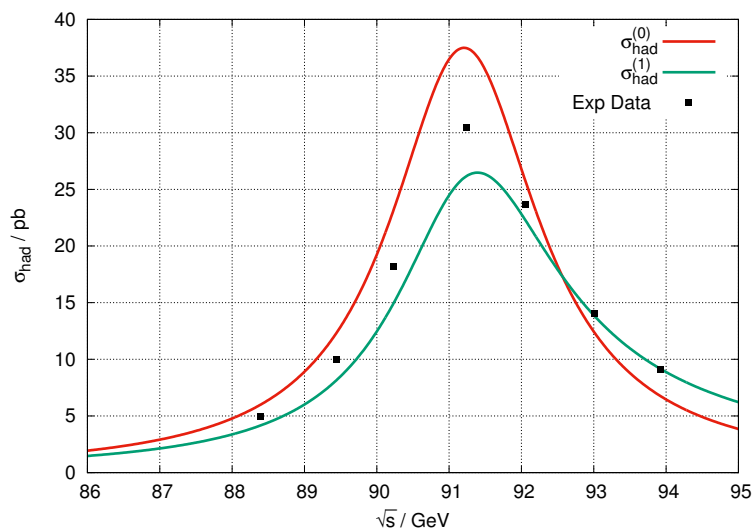


Figure 3.6: The total cross-section of $e^- + e^+ \rightarrow \text{hadrons}$

3.3 Higher-order QED correction

Before moving on to the conclusion, let's have a very brief discussion concerning higher-order QED correction. The analytical formulas for σ_T and A_{FB} have been again taken directly from the consulting material [10] and [5] with the radiators $G(z)$ and $\tilde{H}_e(z)$ are respectively:

$$G(z) = \frac{2\alpha}{\pi}(L_e - 1)(1 - z)^{\frac{2\alpha}{\pi}(L_e - 1) - 1} (1 + \delta_1^a + \delta_2^a) - \frac{\alpha}{\pi}(1 + z)(L_e - 1) + \frac{\alpha^2}{2\pi^2} \left\{ X(z) - (1 + z) \left[2 \ln(1 - z)(L_e - 1)^2 + (L_e - 1) \left(\frac{3}{2}L_e + 2\zeta(2) - 2 \right) \right] \right\} \quad (3.3.1)$$

$$\delta_1^a = \frac{\alpha}{\pi} \left(\frac{3}{2}L_e + 2\zeta(2) - 2 \right)$$

$$\delta_2^a = \frac{\alpha^2}{\pi^2} \left[\left(\frac{9}{8} - 2\zeta(2) \right) L_e^2 + \left(-\frac{45}{16} + \frac{11}{2}\zeta(2) + 3\zeta(3) \right) L_e - \frac{6}{5}\zeta(2)^2 - \frac{9}{2}\zeta(3) - 6\zeta(2) \ln 2 + \frac{3}{8}\zeta(2) + \frac{19}{4} \right]$$

$$X(z) = \left(-\frac{1+z^2}{1-z} \ln z + \frac{1+z}{2} \ln z + z - 1 \right) L_e^2 + \left[\frac{1+z^2}{1-z} \left(Li_2(1-z) + \ln z \ln(1-z) + \frac{7}{2} \ln z - \frac{1}{2} \ln^2 z \right) + \frac{1+z}{4} \ln z^2 - \ln z + \frac{7}{2} - 3z \right] L_e + (1+z) \left[\frac{3}{2} Li_3(1-z) - 2S_{1,2}(1-z) - \ln(1-z) Li_2(1-z) - \frac{1}{2} \right] + \frac{1+z^2}{1-z} \left(-\frac{1}{6} \ln^3 z + \frac{1}{2} \ln z Li_2(1-z) + \frac{1}{2} \ln^2 z \ln(1-z) - \frac{3}{2} Li_2(1-z) - \frac{3}{2} \ln z \ln(1-z) + \zeta(2) \ln z - \frac{17}{6} \ln z - \ln^2 z \right)$$

$$H_e(z) = \frac{2\alpha}{\pi} L_e (1 - z)^{\frac{2\alpha}{\pi} L_e - 1} \delta^b - \frac{\alpha}{\pi} L_e (1 + z) + \frac{\alpha^2}{\pi^2} L_e^2 \left\{ -\frac{1+z^2}{1-z} \ln z - \frac{1+z}{2} \ln [z(1+z)^4] - \frac{5z+1}{2} + \frac{(1-z)^3}{2z} + \frac{(1-z)^2}{\sqrt{z}} \left(\arctan \frac{1}{\sqrt{z}} - \arctan \sqrt{z} \right) \right\} \quad (3.3.2)$$

$$\delta^b = 1 + \frac{3\alpha}{2\pi} L_e + \frac{\alpha^2}{\pi^2} L_e^2 \left(\frac{9}{8} - 2\zeta(2) \right)$$

Here, we have introduced $\zeta(n)$, $Li_n(x)$, and $S_{n,p}(x)$ which are respectively the Riemann zeta function, the polylogarithm (also known as Jonquière's function), and the Nielsen generalized polylogarithm.

With the formulas of the radiators in (3.3.1) and (3.3.2), we have the forward-backward asymmetry and the total cross-section are:

$$\sigma_T^{(2)}(s) = \int_{z_0}^1 dz G(z) \sigma_T^{(0)}(zs) \quad (3.3.3)$$

$$A_{FB}^{(2)}(s) = \frac{1}{\sigma_T(s)} \int_{z_0}^1 dz \frac{4z}{(1+z)^2} \tilde{H}_e(z) \sigma_{FB}^{(0)}(zs) \quad (3.3.4)$$

Notice that higher-order QED correction formulas were labelled with the upper index (2). Now, we could see that there is no cut-off parameter ε within the formulas of the radiators. However, for numerical evaluation, if we leave the upper limit of the integral to be $z = 1$, the results may converge very slowly. Hence, we shall utilize the strategy used in the previous subsection which is to change the upper limit of the integral from $z = 1$ to $z = 1 - \varepsilon$ and again choose ε to be small enough ($\varepsilon \ll 1$). For the input parameters:

$$\begin{aligned} m_\mu &\simeq 0.0 \text{ GeV}, & m_Z &= 93.0 \text{ GeV}, & \Gamma_Z &= 2.5 \text{ GeV}, \\ G_\mu &= 1.166344 \cdot 10^{-5} \text{ GeV}^{-2}, & \alpha &= \frac{1}{137.03604}, & \sin^2 \theta_W &= 0.23, \end{aligned}$$

We have the numerical results with higher-order QED correction in comparison with those in [5] presented in table (3.3). Once again, we have the input parameter $m_\mu = 0$ GeV, it means that massless fermion approximation was utilized. Also, in this case we used the coupling constants as indicated in formulas (3.2.7) and (3.2.8).

\sqrt{s}	[0] ($\varepsilon = 10^{-2}$)	[0] ($\varepsilon = 10^{-4}$)	[0] ($\varepsilon = 10^{-6}$)	[0] ($\varepsilon = 10^{-8}$)	[5]
82.0	-30.840	-41.598	-44.129	-44.373	-54.63
92.5	-12.847	-5.019	-3.930	-3.511	-3.643
93.0	-8.817	-1.518	-0.554	-0.261	0.289
93.5	-5.166	1.387	2.339	2.569	3.760
100.0	7.064	12.613	14.786	15.592	20.49

Table 3.3: Comparison with table 9 of to [5] for $e^- + e^+ \rightarrow \mu^- + \mu^+$ with higher-order QED correction in percent

Unfortunately, in this case, we are not able to see the limit as the numerical results oscillate slightly for small values of ε . This might be due to the incapability of the program chosen to perform numerical integration (Mathematica 10). In figure (??), we could also see the numerical results do not well converge in the case of higher-QED correction comparing to the one for QED correction.

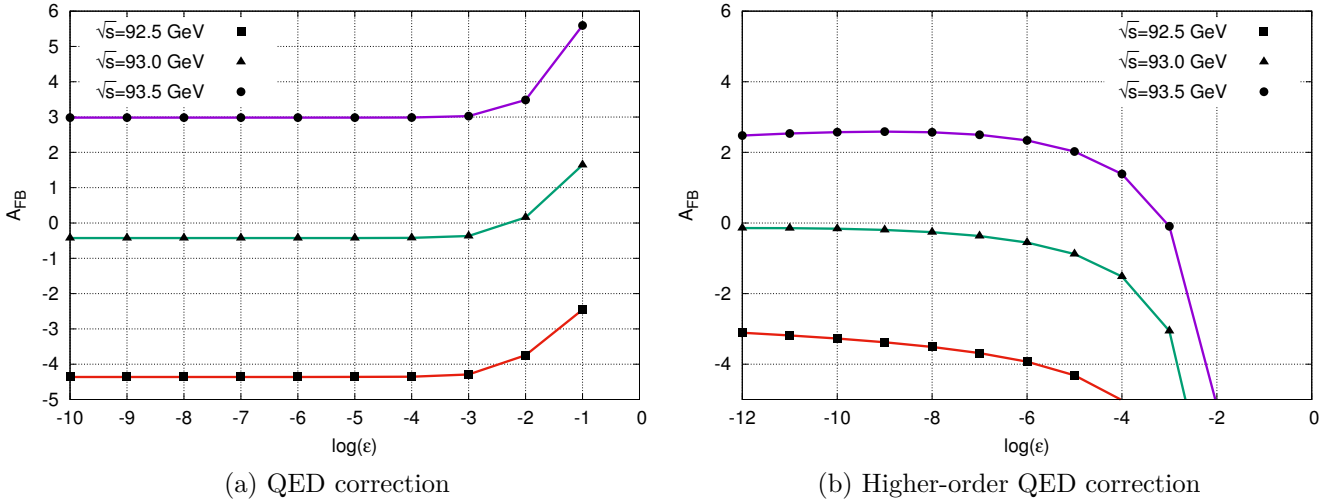
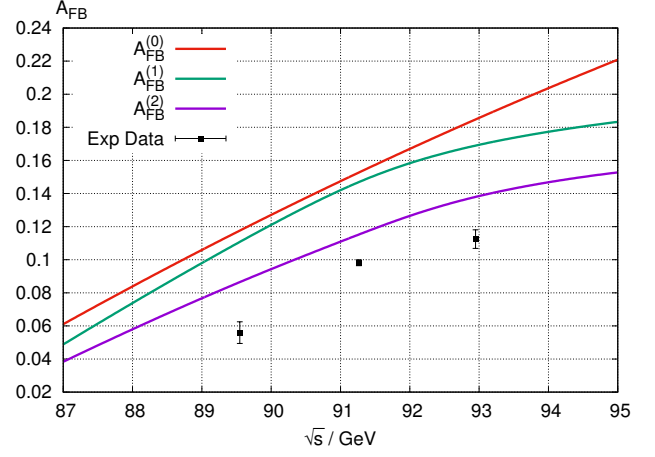
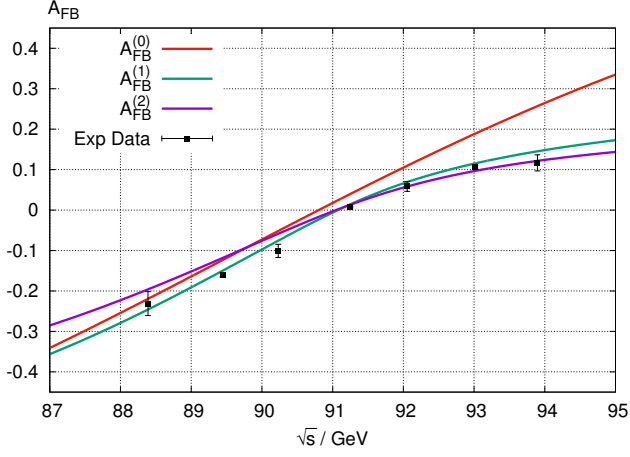


Figure 3.7: The numerical values of A_{FB} with respect to $\log(\epsilon)$ in two cases

Nevertheless, we could still see that the results are mostly of the same scale and the differences between our numerical results are not quite large. Hence, we chose $\epsilon = 10^{-8}$ to plot some of the results to see the difference between QED correction and higher-order QED correction as in figure (3.8).

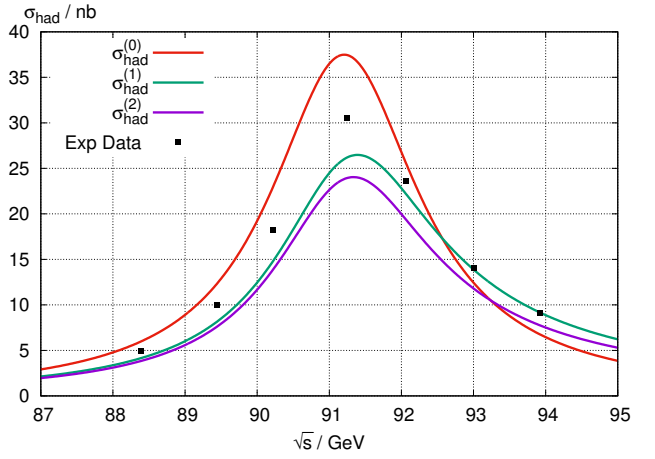
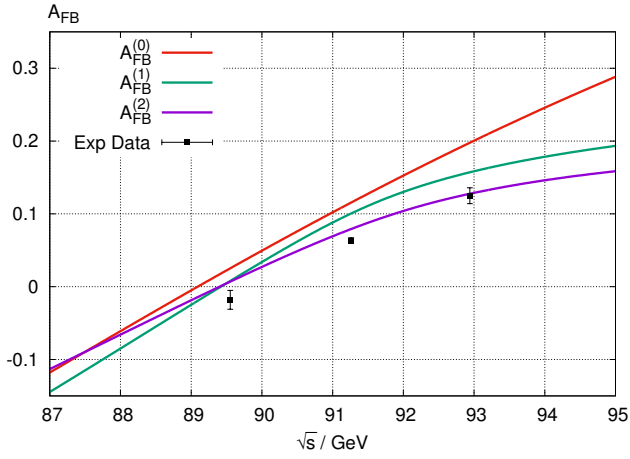
Although, the two results still does not match for the cases of figure (3.8b), (3.8c), and (3.8d), the theoretical results with higher-order QED correction seem to be in better agreement with experimental ones particularly for the forward-backward asymmetry of b-quark and c-quark.

Here, we have to stress that our results for higher-order QED correction ($\sigma_T^{(2)}(s)$ and $A_{FB}^{(2)}(s)$) are likely to be wrong since they did not well converge. The pattern of the results is, however, consistent with the ones presented in [8] where significant differences between the theoretical predictions and the experimental data were observed for the case of b-quark.



(a) Forward-backward asymmetry of $e^- + e^+ \rightarrow \mu^- + \mu^+$

(b) Forward-backward asymmetry of $e^- + e^+ \rightarrow b + \bar{b}$



(c) Forward-backward asymmetry of $e^- + e^+ \rightarrow c + \bar{c}$

(d) Total cross-section of $e^- + e^+ \rightarrow \text{hadrons}$

Figure 3.8: Results for higher-order QED correction with $\varepsilon = 10^{-8}$ GeV

Conclusion and outlook

Conclusion

From what we have done so far, some important conclusions could be drawn for the scattering process of type $e^- + e^+ \rightarrow f + \bar{f}$ ($f \neq e$):

- First, for $f = \mu^-$ as could be seen from the calculation in the first two chapters with the inclusion of Z -boson (in addition to photon) as a mediator—a profound difference between SM and QED, we could theoretically predict the forward-backward asymmetry of muon in pair creation which does not appear in QED.
- Also, in the case $f = \mu^-$ but at low energy scale, results of the two theories come close to each other as presented in chapter 2. This confirms that QED is in fact an approximate theory of SM in the range of low energy.
- Regarding initial state QED correction, it significantly affects the results of all the quantities of interest. Particularly, it contributes to the 40%-reduction in the height of Z -peak for muon.
- Finally, we could see that by considering also effects of soft photon emission using initial state QED correction (and even higher-order QED correction), our theoretical predictions seem to be in better agreement with the experimental results especially for the case $f = \mu^-$. This means that for a more precise comparison with experimental data, initial state QED correction should definitely be taken into account.

Outlook

For further development, there are some crucial improvements required:

- In order to make better progress, it is crucial to increase the accuracy of the numerical integration with better strategy. In particular, the results of higher-order QED correction have to be re-examined.
- For cases where $f = b$ or $f = c$, a more thorough final state QCD corrections might be needed so as to enhance the matching between theoretical and experimental results.
- Another fascinating direction of development is to proceed with higher energy range. In that case, we will be able to consider also heavier quarks like $f = t$ for instance.

- More interestingly, we could actually go beyond the SM for example to demanding the Lagrangian to be symmetric under an extra group $U(1)'$. As a result, a new term with an associated gauge boson mediator called Z' -boson should be added to the Feynman amplitude for all the results to be re-deduced.

Bibliography

- [1] M. Steinhauser, Übungen zu strahlungskorrekturen in eichtheorien, Herbstschule für Hochenergiephysik, 2003, <http://maria-laach.physik.uni-siegen.de/downloads/files/2003/Steinhauser-2003.pdf>.
- [2] D. Griffiths, Introduction to elementary particles, 2nd, revised ed. (Addison-Wesley Pub. Co, 2008).
- [3] M. Kardar, Statistical physics of particles, 1st ed. (Cambridge University Press, 2007).
- [4] J. Kuipers et al., Comput. Phys. Commun. 184 (2013) 1453, 1203.6543.
- [5] M. Bohm et al., Geneva 1989, Proceedings, Z physics at LEP 1, vol. 1* 203-234 and CERN Geneva - TH. 5536 (89,rec.Nov.) 36 p, 1989.
- [6] M. Bohm and W. Hollik, Phys. Lett. B139 (1984) 213.
- [7] D. Zhang, Muon pair production in e^+e^- collisions at the Z resonance, PhD thesis, Amsterdam U., 1994.
- [8] SLD Electroweak Group, DELPHI, ALEPH, SLD, SLD Heavy Flavour Group, OPAL, LEP Electroweak Working Group, L3, S. Schael et al., Phys. Rept. 427 (2006) 257, arXiv:hep-ex/0509008.
- [9] P. Uwer, EasyNData: A simple tool to extract numerical values from published plots, 2007, arXiv:0710.2896.
- [10] D.Yu. Bardin et al., Geneva 1989, Proceedings, Z physics at LEP 1, vol. 1* 89-127., 1989.
- [11] M.E. Peskin and D.V. Schroeder, An Introduction to quantum field theory, 1st ed. (Addison-Wesley Pub. Co, 1995).
- [12] Particle Data Group, K. Hagiwara et al., Phys. Rev. D66 (2002) 010001.
- [13] W. Hollik, High-energy physics. Proceedings, 17th European School, ESHEP 2009, Bautzen, Germany, June 14-27, 2009, 2010, arXiv:hep-ph/1012.3883.